# On Periodic Gene Expression in Budding Yeast

**Rainer Machné**[1,2,*], **Douglas B. Murray**[3,4], **Stephan H. Bernhart**[5], **Ilka M. Axmann**[1], **Peter F. Stadler**[5,6,7,8,9]

***For correspondence:**
machne@hhu.de (RM);
mabawsa@gmail.com (DBM)

[1]Institute for Synthetic Microbiology and; [2]Institute for Quantitative and Theoretical Biology, Heinrich Heine University, D-40225 Düsseldorf, Germany; [3]Lakeland University Japan, Shinjuku-ku, Tokyo 160-0022, Japan; [4]University of Maryland Global Campus—Asia, Yokota Air Base, Fussa-shi, Tokyo 197-0001, Japan; [5]Bioinformatics Group, Department of Computer Science, Interdisciplinary Center for Bioinformatics, Universität Leipzig, Härtelstraße 16-18, D-04107 Leipzig, Germany; [6]Max Planck Institute for Mathematics in the Sciences, Inselstraße 22, D-04103 Leipzig, Germany; [7]Institute for Theoretical Chemistry, University of Vienna, Währingerstraße 17, A-1090 Wien, Austria; [8]Facultad de Ciencias, Universidad Nacional de Colombia, Sede Bogotá, Colombia; [9]Santa Fe Institute, 1399 Hyde Park Road, Santa Fe NM 87501, USA

## Abstract

Metabolic oscillation percolate throughout cellular physiology. The transcriptome oscillates between gene cohorts encoding for biosynthesis and growth, and for catabolism and stress response. However, long protein half-lives dampen effects on protein abundance, and the function of periodic transcription remains elusive. To test three prevailing hypotheses, we performed RNA-seq analysis during a dynamic state of the system, just preceding a bifurcation of system dynamics to a longer period. A few enzymes with short protein half-live and high transcript abundance amplitude could play a direct role in metabolic dynamics (hypothesis H1), e.g., carbonic anhydrase, sulfate uptake and the glyoxylate cycle. Substantial changes in the relative duration of expression of the antagonistic cohorts precede the bifurcation, supporting the idea of a function in cellular resource allocation (H2). The pulse-width modulation model, a mathematical formulation of this idea, explains the dependence of the cycle period on the culture growth rate. This pulse-like model of cell growth provides a first theoretical framework, where the phenomenon is understood as a mechanism of cellular resource allocation and protein homeostasis. The universal temporal program of transcription encodes the spatial structure of the cell, and we further suggest a function in pattern formation of the growing cell (H3).

## Introduction

When yeast cultures are grown to a high cell density they tend to show collective metabolic dynamics, alternating between phases of high oxygen consumption (HOC) and low oxygen consumption (LOC). Numerous studies on continuously grown yeast have shown that stable oscillatory dynamics propagate throughout the metabolome, transcriptome and impinge on chromatin organization. The cycle period is dependent on growth conditions and the strain employed. However, under equivalent growth conditions experimental data can be categorized into long ($\tau_{osc} = 4\,\mathrm{h}–5\,\mathrm{h}$) or short period cycles ($\tau_{osc} = 0.7\,\mathrm{h}–1\,\mathrm{h}$; peculiar to the diploid strain IFO 0233). The cell division cycle (CDC) is tightly or loosely coupled with the long or short period cycles, respectively. The phe-

nomenon is considered a model system for circadian cell biology in the absence of a circadian clock (***Causton et al., 2015***; ***Mellor, 2016***), or, more generally, for multi-scale coherence of cellular processes (***Sonnleitner et al., 1997***; ***Lloyd and Murray, 2007***; ***Aon et al., 2008***). Long period cycles were explained by a partial synchronization of the CDC, revealing the asymmetry of the yeast budding cycle (***Küenzi and Fiechter, 1969***; ***von Meyenburg, 1969a***; ***Münch et al., 1992***; ***Bellgardt, 1994***; ***Hjortso and Nielsen, 1995***; ***Duboc and von Stockar, 2000***; ***Futcher, 2006***). ***Satroutdinov et al.*** (***1992***) then observed much shorter periods in IFO 0233, which questioned these prior models, including a causal role of the glycogen storage cycle.

Despite these differences in periods and metabolic flux patterns, a similar temporal program of gene expression is observed in both short period (IFO 0233) and long period experimental systems (***Machné and Murray, 2012***). Both show maxima and minima of the cellular ATP/ADP ratio during the HOC and early LOC phases, respectively (***von Meyenburg, 1969b***; ***Satroutdinov et al., 1992***; ***Xu et al., 2004***; ***Müller, 2006***; ***Machné and Murray, 2012***; ***Amariei et al., 2014***). Global remodeling of promoter and gene body nucleosome organization occurs during the late LOC phase (***Amariei et al., 2014***; ***Nocetti and Whitehouse, 2016***). During HOC, transcription progresses from a ribosome biogenesis cohort (`Ribi`) and cytoplasmic ribosomal protein genes (`RP`), to amino acid synthesis genes (`AA`) and mitochondrial ribosomal protein genes (`mtRP`) at the transition to LOC. During the LOC phase, transcripts of a large group of stress-response and catabolic proteins (`S/C`) peak. In IFO 0233, the latter overlaps with expression of the `mtRP` cohort, while in long period systems these are separated (***Machné and Murray, 2012***). Several hypotheses on putative functions of the temporal program have been suggested. The functional profiles of co-expressed cohorts match metabolic activity, and the initial hypothesis was a "just-in-time" model of gene expression (**H1**), where enzymes are expressed when required within the metabolic cycle (***Klevecz et al., 2004***; ***Tu et al., 2005***; ***Murray et al., 2007***). However, protein half-lives in yeast are now thought to be much longer than initially reported (***Christiano et al., 2014***). This dampens the effect of periodic transcript on protein abundances (***Lück et al., 2014***). Indeed recent proteomic studies found no (**preprint:** ***Feltham et al.*** (***2019***)) or only few (***O' Neill et al., 2020***) periodic protein abundances in long period systems. Thus, ***Feltham et al.*** (***2019***) suggest a null hypothesis (**H0**) where periodic mRNA synthesis and degradation produce no significant costs and are a side-effect of the metabolic states the cells traverse. ***Slavov and Botstein*** (***2011***) and ***Burnetti et al.*** (***2016***) suggested an alternative hypothesis (**H2**), based on the observation that the relative duration of the LOC phase varies strongly while HOC phase duration only subtly changes with growth rate. This would result in different absolute abundances of the proteins from HOC- and LOC-specific co-expression cohorts and could underlie growth rate-dependent cellular resource allocation (***Maaløe, 1979***; ***Molenaar et al., 2009***). And finally, the association of protein biosynthesis with HOC phase and of protein aggregation and autophagy with LOC phase led to suggestions of a conserved eukaryotic cell growth cycle with a main role in protein homeostatis (**H3**) (***von Meyenburg, 1969b***; ***Klevecz, 1976***; ***Klevecz et al., 2004***; ***Lloyd and Murray, 2007***; ***Murray et al., 2007***; ***Slavov et al., 2012***; ***O' Neill et al., 2020***).

To test these (non-exclusive) hypotheses, we performed strand-specific RNA-sequencing in high temporal resolution during a dynamic state of the short period cycle of the strain IFO 0233; after a multi-generational drift of period and amplitudes and just preceding a distinct bifurcation to longer but unstable periods. Global system variables, such as ATP flux and proton export, oscillated, confirming the cell-wide nature of the cycle. Only few proteins with short half-lives and high transcript abundance amplitudes are compatible with **H1**, and their metabolic substrates dynamically changed over the bifurcation. The bulk of the protein coding transcriptome followed the conserved program and a pronounced shift from HOC phase-specific to LOC phase-specific transcript abundance peaks occurred within just two cycles, compatible with **H2**. A mathemtical formulation of H2, the pulse-width modulation (PWM) model, reproduces the observed relations of cycle periods and of relative proteome fractions to growth rate.

# Results

## Long Transients and a Bifurcation to Longer Periods

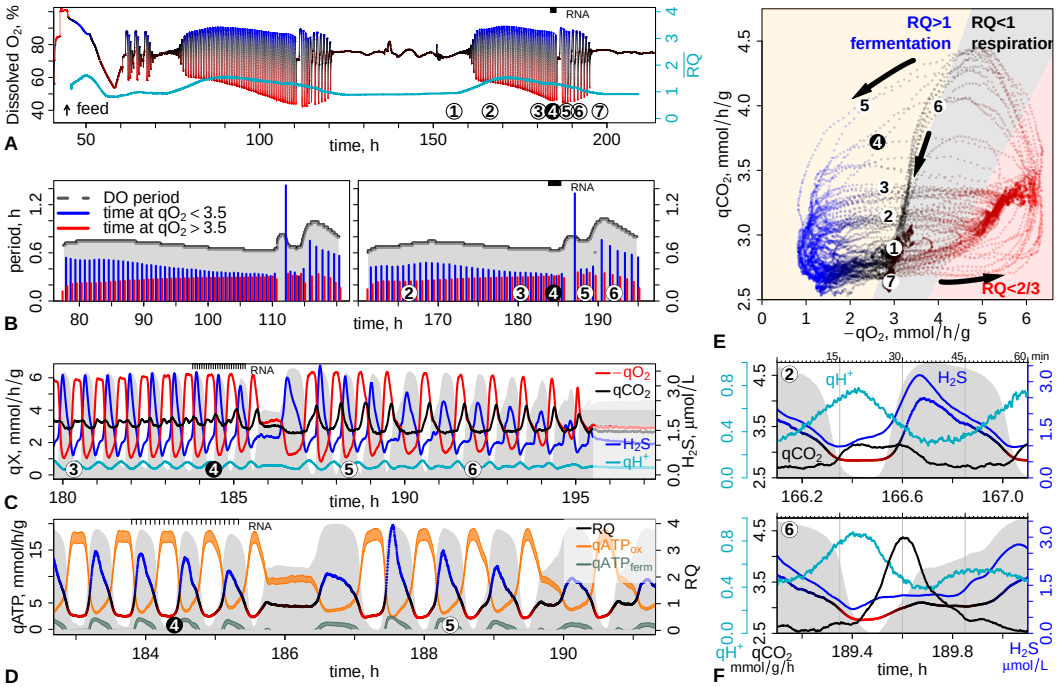


**Figure 1. Complex Dynamics: Slow Transients and a Sudden Bifurcation.** Metabolic dynamics during continuous culture of the budding yeast strain IFO 0233: panel A shows the full recorded time-series of the culture, and panels B–E zoom in on the time axis; bullet points P1–P7 serve as a guide between panels and are discussed in the text. The gray backgrounds show the dissolved $O_2$ concentration (see A for axis) and serves as a reference to oscillation phase. **A:** Dissolved $O_2$ (DO) measurement from the start of continuous feeding (dilution rate $\phi = 0.089\,\mathrm{h}^{-1}$). Line colors are derived from the respiratory quotient RQ (D) and indicate phases of high $O_2$ consumption (HOC: red) and low $O_2$ consumption (LOC: blue). The cyan line and right axis show the temporal mean $\overline{\mathrm{RQ}}$, a moving average over ca. 10 h. **B:** The cycle periods for the dynamic transients were derived from a Wavelet transform of the DO signal and the phase lengths are the time spans of each cycle where oxygen uptake ($-q_{O_2}$) stayed below (red) or above (blue) $3.5\,\mathrm{mmol/h/g_{DCW}}$. **C:** Zoom on P3–P6 for measured metabolic rates and concentrations; $q_{O_2}$, $q_{CO_2}$ and $H_2S$ were measured in the offgas of the reactor, corrected for the measurement delay and $H_2S$ concentration was derived via its solubility. Proton export ($q_{H^+}$) was calculated from the NaOH addition rate. **D:** Zoom on P4–P5 for calculated rates. The respiratory quotient (RQ) and ATP production rates by respiration ($q_{ATP\,ox}$) or by fermentation ($q_{ATP\,ferm}$) were calculated from $q_{O_2}$ and $q_{CO_2}$, ranges of $q_{ATP}$ show values for pure glucose oxidation and fermentation, or pure fermentation of glucose and oxidation of only ethanol. The RQ color gradient serves as a reference in (A, E). **E:** Phase portrait of $q_{O_2}$ and $q_{CO_2}$ over the time range indicated by bullet points in (A); colored by RQ (D), arrows indicate time direction; background colors indicate RQ ranges. **F:** One-hour snapshots at different times (bullet points 2 and 5). Data are indicated by colored axes and labels, except for RQ which is shown without axis but color-coded (red-black-blue) as in D and E.

Previously, short-period oscillatory dynamics have been used to elucidate the transcriptome dynamics of continuously grown yeast (***Klevecz et al., 2004***; ***Li and Klevecz, 2006***). Here we observed more complex spontaneous dynamic transients (Fig. 1A, S4, S6), i.e., two self-similar time-series of respiratory dynamics where each event lasted $30\,\mathrm{h}$–$40\,\mathrm{h}$ and spanned multiple cell cycles. We calculated metabolic rates (Appendix A) to characterize these dynamics. During the majority of these transients typical oscillatory periods for the yeast strain IFO 0233 ($0.6\,\mathrm{h}$–$0.7\,\mathrm{h}$ (Fig. 1B-C) were observed. The culture cycled between a phase of low oxygen consumption (LOC, here: $-q_{O_2} < 3.5\,\mathrm{mmol/h/g_{DCW}}$) and fermentation (respiratory quotient $\mathrm{RQ} = \frac{q_{CO_2}}{-q_{O_2}} > 1$), and a phase of high oxygen consumption (HOC). During the HOC phase, RQ decreased below $\frac{2}{3}$, i.e., the stoichiometry of complete ethanol oxidation (Fig. 1D), consistent with re-uptake of ethanol (***Satroutdinov et al.,***

***1992***) but pointing to additional contributions to $CO_2$ turnover. The temporal mean $\overline{\mathrm{RQ}} > 1$ (Fig. 1A) indicates net fermentation during the dynamic state, but stoichiometric estimation of ATP production rates $q_{\mathrm{ATP}}$ showed that fermentation did not contribute significantly to overall ATP turnover (Fig. 1D). The estimated ATP turnover rates were in phase with previously measured ATP/ADP ratios, peaking in early to mid HOC phase (***Machné and Murray, 2012***; ***Amariei et al., 2014***). The concentration of $H_2S$ peaked at $\approx 3\,\mu\mathrm{M}$ with a sharp increase upon transition to LOC (Fig. 1C, F), consistent with its release during amino acid biosynthesis in this transition phase (***Murray et al., 2007***) and its suggested role in population synchronization (***Murray et al., 2003***).

Both transients were characterized by a gradual increase of amplitudes and a decrease of the period (Fig. 1A, B, E, S4, S6). LOC phase duration ($\tau_{loc}$) decreased stronger then the total period, while HOC phase duration ($\tau_{hoc}$) increased (bullet points P2-P3, Fig. 1A, B, S4). A plateau of $q_{CO_2}$ was split into two distinct peaks flanking the HOC phase (P3-P4, Fig. 1C–E). The first $q_{CO_2}$ peak vanished and a sharper peak appeared at the transition to LOC phase, immediately preceding a distinct bifurcation of system dynamics. An additional phase first appeared at this bifurcation; metabolism was respiratory (RQ $\approx 1$) and all parameters remained at intermediate values for about one full oscillation cycle (time $t = 186\,\mathrm{h}$), Fig. 1C, S5). The $H_2S$ peak was delayed and preceded the following long and pronounced LOC phase. The system then fell back to a shorter period, but $q_{CO_2}$ remained phase-delayed and with higher amplitude (P5, Fig. 1C–F). Finally, the period increased to $\tau_{osc} \approx 1\,\mathrm{h}$, and the pause between HOC and LOC phases re-appeared as a shoulder peak, again at RQ $\approx 1$ and flanked by pulses of $CO_2$ and $H_2S$ release (P6, Fig. 1C–F).

In summary, we confirmed that the metabolic cycle reflects a cell-wide phenomenon. Here, a gradual uncoupling of $CO_2$ release from respiratory activity preceded a bifurcation of system dynamics. A new phase appeared at the transition from HOC to LOC, characterized by purely respiratory metabolism. Low but purely respiratory activity at RQ $\approx 1$ is characteristic of the LOC phase in CDC-coupled systems (***Münch et al., 1992***). This bifurcation was accompanied by a pulse of $CO_2$ release before, and a shifted pulse of $H_2S$ release after the intermediate RQ $\approx 1$ phase.

## A Universal Temporal Program

### Non-Coding Transcription is Biased to LOC Phase.

Numerous time series of the protein-coding transcriptome have revealed a universal temporal program of defined transcript cohorts but with periods ranging from $40\,\mathrm{min}$ to $7.5\,\mathrm{h}$ (***Machné, 2017***; ***Mellor, 2016***). Neither the effect of transient states of the oscillation nor non-coding transcription have been studied yet. We sampled for RNA-seq analysis in high temporal resolution ($4\,\mathrm{min}$) for 2.5 cycles, just preceding the bifurcation of system dynamics (P4 in Fig. 1). The strand-specific sequencing reads were mapped to the reference genome (strain S288C, R64-1-1), yielding reads for $76\,\%$ of the genome (Fig. S8A). A similarity-based segmentation algorithm (***Machné et al., 2017***) yielded ca. 37k segments (Fig. S8D), each a putative individual transcript. All segments were classified by their oscillation p-values, calculated with the `rain` package (***Thaben and Westermark, 2014***), and by their overlaps with annotated genome features (Tab. S2). 4,489 segments were classified as open reading frame (ORF) transcripts; 3,378 of these showed oscillation and reproduced the previously characterized temporal sequence (Fig. 2A; ***Machné and Murray*** (***2012***)). Oscillating non-coding (811 of 9,051) and antisense (232 of 569) segments predominantly peaked in the LOC phase. Very short and weakly expressed segments were removed from further analyses, the remaining 11k segments (Fig. S8G–I) were clustered into ten co-expressed cohorts, and these were sorted and colored by their peak phase (Fig. S9–S11). These ten cohorts can be further classified (Fig. S9C) into two groups of five clusters. The first group (Fig. 2B) comprises of longer segments with high amplitudes, and most assigned to protein-coding genes (Fig. S10). The second group of clusters (Fig. 2C) contain shorter and weakly expressed segments with lower amplitudes, mostly non-coding and peaking during the LOC phase (Fig. S11).

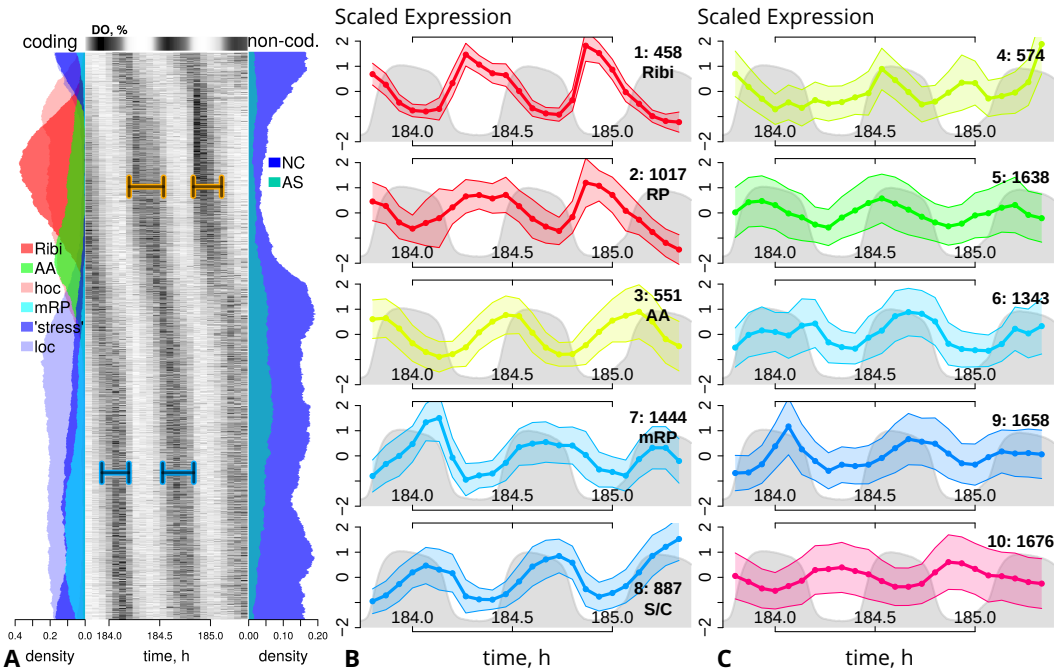


**Figure 2. RNA-seq Segmentation and Clustering. A:** phase-ordered heatmap of the time-courses of segments with oscillating abundance levels (6344 segments at $p_{\text{rain}} < 0.05$, Fig. S8E)). The dissolved $O_2$ (DO, %) is shown as a color gradient (black: high DO) on the top axis. Left and right panels show local densities (circular moving average of counts over 1/10 of the total number) of segments overlapping with previously defined (***Machné and Murray, 2012***) classes of coding genes (left: Ribi, ribosomal biogenesis and cytoplasmic ribosomal proteins; AA: amino acid synthesis; mRibi: mitochondrial genes, incl. ribosomal proteins; stress: catabolic and protein homeostasis genes), or non-coding segments (right: AS, antisense to ORF; NC, no overlap with any annotated transcribed feature). **B:** time series of the five major periodic co-expression cohorts. Segment time-courses (mean RPM) were normalized to mean of 0 and divided by their standard deviation (R function `scale`). The mean of each cluster is shown as a solid line with points indicating the sampling times, and standard deviations as transparent ranges; the legends indicate the cluster label, the number of segments in the cluster and the posterior functional cohort assignment. The gray background indicates the dissolved $O_2$ (DO) concentration. **C:** time series for the cohorts 4, 5, 6, 9, 10, which comprise mostly segments without or little overlap with coding regions; plotted as described for (B).

## The Same "Functio-Temporal" Program Runs at Different Time Scales.

Gene Ontology (GO) enrichment analysis of the protein coding-cohorts (Fig. 3A and S12) recapitulates previous results (***Klevecz et al., 2004***; ***Machné and Murray, 2012***). The ribosomal biogenesis regulon (***Jorgensen et al., 2004***) peaks in early to mid HOC phase (cluster 1: `Ribi`), followed by clusters encoding for cytoplasmic ribosomal proteins (cluster 2: `cRP`), and amino acid biosynthetic pathways (cluster 3: `AA`) at the transition to LOC phase. During the LOC phase, mitochondrial proteins, including mitochondrial ribosomal proteins (cluster 7: `mRP`) are co-expressed with a regulon associated with stress response (***Gasch et al., 2000***; ***Brauer et al., 2005***) and G1 phase (***O'Duibhir et al., 2014***). The latter comprises of proteins involved in the general stress response (chaperones) and in carbohydrate, fatty acid and protein catabolism (cluster 8: `S/C`). We used this clustering to re-analyze seven data sets from different strains and conditions and with periods ranging from $40\,\text{min}$ to $7.5\,\text{h}$ (***Li and Klevecz (2006)***; ***Tu et al. (2005)***; ***Chin et al. (2012)***; ***Kuang et al. (2014)***; ***Wang et al. (2015)***; ***Slavov et al. (2011)***; Fig. S13–S15). This meta-analysis reveals common patterns. A temporally constrained program ($0.5\,\text{h}$–$2\,\text{h}$) leads from `Ribi`/`cRP` *via* `AA` to `mRP`, ending with the transition from HOC to LOC phase. Variation in the total period are mostly reflected by increased duration of the LOC phase and the associated `S/C` cohort expression. Very similar temporal patterns can be observed in six distinct cell cycle arrest & release experiments (Fig. S16) (***Orlando et al., 2008***; ***Bristow et al., 2014***).

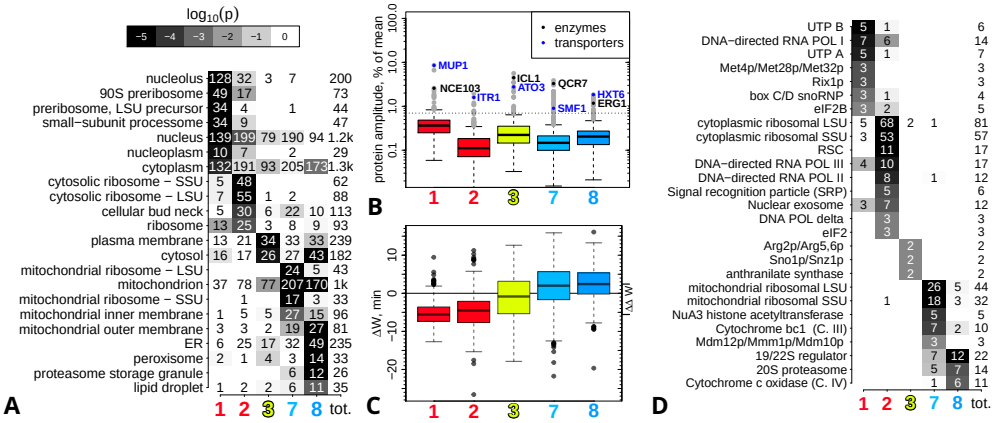


**Figure 3. A Universal Temporal Program. A:** Sorted cluster enrichment profiles for the GO category "cellular component". The p-values were calculated by cumulative hypergeometric distribution tests and are shown as gray-scale. Only categories with $p < 0.001$ (white text) and more then 10 genes in one of the clusters are shown. See Figure S12 for all clusters and GO categories. **B:** Box-plots of cluster distributions of predicted relative protein amplitudes $A_{\text{protein}}$, estimated from transcript amplitudes and protein half-lives (Fig. S17). The horizontal line indicates the the top 100 oscillators listed in Table S3. The top predicted oscillators of class enzyme or membrane transporter of each cluster are indicated. **C:** Box-plots of cluster distributions of peak-width changes. $\Delta W = W_2 - W_1$ is the difference of the peak widths (Fig. S20) between the second and first full expression cycle, and $\Delta\Delta W$ is the difference of $\Delta W$ medians of clusters 1 and 8. **D:** Cluster enrichment profile ($p_{\text{sort}} = 0.01$) of protein complexes in the CYC2008 annotation (***Pu et al., 2009***), colored as in (A). For a comprehensive picture of complex expression, the segment with the best overlap (highest Jaccard index $J > 0$) was considered for each coding gene. See Figure S21 for all clusters.

## Testing Hypotheses on Putative Functions of the Temporal Program

Next, we analzyed the three prevailing hypotheses on putative functions of this universal temporal program; the *just-in-time production* hypothesis (H1), the *resource allocation* hypothesis (H2), and the *protein homeostasis* hypothesis (H3).

### Carbonic Anhydrase and the Glyoxylate Cycle are Novel Feedback Candidates.

The temporal order of mRNA abundances makes intuitive sense as a just-in-time gene expression program (**H1**) coordinated with metabolic events (***von Meyenburg, 1969b***; ***Klevecz et al., 2004***; ***Tu et al., 2005***; ***Murray et al., 2007***; ***Machné and Murray, 2012***). However, oscillations on transcript level are dampened by long protein half-lives. Thus, we estimated relative protein amplitudes from our RNA abundance time series and from protein half-life data by ***Christiano et al.*** (***2014***), using a mathematical model of periodic gene expression by ***Lück et al.*** (***2014***). Most proteins are predicted to vary by $0.1\,\%$–$0.5\,\%$ of their mean abundance (Fig. 3B and S17). Only 23 proteins have predicted relative protein amplitudes $\geq 2\,\%$; and oscillators are enriched in the `Ribi` and `AA` cohorts (Fig. S18). These low amplitudes can hardly be argued to have a strong effect on metabolic dynamics, but the model is based on sine approximations of transcript time series and protein half-lives measured in asynchronous conditions; it may understimate amplitudes and it completely neglects potential effects of induced protein degradation. The top 100 list contains several cell wall proteins, nutrient transporters, transcription factors, and some metabolic enzymes (Fig. S17, Tab. S4 and Dataset S3). Several proteins of the sulfate uptake pathway (MET genes) are expressed in `Ribi`, peaking prior to the pathway intermediate $H_2S$ at the HOC/LOC transition (Fig. 1). The carbonic anhydrase (NCE103, in `Ribi`) catalyzes the interconversion of carbon dioxide and bicarbonate ($CO_2 + H_2O \leftrightarrow HCO_3^- + H^+$), and is essential in aerated cultures (***Aguilera et al., 2005***). During the second sampled cycle the `Ribi` cohort was downregulated early (Fig. 2A, Fig. 3C) and this correlated with the appearance of the $CO_2$ and the delay of $H_2S$ release pulses at transition to LOC (Fig. 1C–F). Both, $CO_2$ and $H_2S$, are substrates of biosynthetic metabolism and several key enzymes of biosynthesis are among our top oscillators, notably three enzymes of the glyoxylate cycle (ICL1, CIT2, MDH2); all expressed with the

AA cohort. These short-lived enzymes could be involved in gating the transition from the catabolic to the anabolic phase of the cycle. The phase shifts of $CO_2$ and $H_2S$ release at the bifurcation (Fig. 1F) may indicate an imbalance between catabolic and anabolic flux. In Figure S19 we develop a speculative but testable, integrative picture of this switch.

## Resource Allocation by Pulse-Width Modulation.

Most proteins are too stable to be affected by oscillatory transcript abundances. ***Slavov and Botstein*** (***2011***) and ***Burnetti et al.*** (***2016***) suggested an alternative interpretation of periodic transcription. Variation of the relative times spent in HOC- and LOC-specific transcription states could serve to tune steady-state protein abundances (**H2**). The LOC phase duration decreases with increasing growth rates, while HOC phase duration remains approximately constant or even slightly increases (***von Meyenburg, 1969a***; ***Slavov and Botstein, 2011***; ***Burnetti et al., 2016***). This would lead to a higher relative biomass fraction of proteins from HOC phase-specific transcripts, i.e. of the Ribi and the cRP cohorts. When growth rate was decreased in dilution rate shift experiments (***Chin et al., 2012***; ***Wang et al., 2015***) the total period increased, as expected. The duration of the expression cohorts increased accordingly, but the increase was higher for the LOC-phase specific cohorts (Fig. S15D). During our experiment a similar shift of the relative times spent with HOC or LOC phase-specific expression occured (horizontal bars in Fig. 2). We quantified and compared the peak widths between the two cycles (Fig. 2A, S20). The S/C cohort peak width increased on average by $\approx 3\,\mathrm{min}$, while the Ribi cohort peak width decreased by $\approx -5\,\mathrm{min}$. This occured without comparable changes in the duration of HOC and LOC phases, i.e., there was no direct coupling of transcript to respiratory dynamics. But it directly preceded the bifurcation and subsequent shift to a longer period with a longer LOC phase.

An increase of ribosome content is directly and causally related to higher growth rates, constituting a fundamental principle of microbial growth physiology (***Schaechter et al., 1958***; ***Waldron and Lacroute, 1975***; ***Koch, 1988***; ***Scott et al., 2010***). This relation is reflected in continuous changes of relative abundances of different transcript and protein classes with growth rate also in budding yeast (***Brauer et al., 2005***; ***Molenaar et al., 2009***; ***Metzl-Raz et al., 2017***). No mechanism for this continous variation of gene expression is known in eukaryotes. A temporal regulation, via continuous changes of the relative durations of LOC and HOC phases, could generate this relation, and we will further evaluate this idea below by a mathematical model.

## The Temporal Program Reflects the Spatial Structure.

The resource allocation model can account for the observed relation of ribosome numbers to growth rate, and the model holds for different periods. However, it offers limited insights for the universal program, the temporal sequence of co-expression cohorts. ***O' Neill et al.*** (***2020***) suggest that the cycle serves to support the energetic demand of protein homeostasis (**H3**), where translation rate is higher in HOC phase, and proteins aggregate and are degraded in LOC phase. Here, we speculate that the temporal program can also be understood within this model, invoking another recent observation. Many large protein complexes form co-translationally, and protein subunits misfold if translated in isolation (***Langdon et al., 2018***; ***Shiber et al., 2018***; ***Schwarz and Beck, 2019***). The GO analysis by the *cellular component* category maps the temporal program onto the spatial structures of the cell (Fig. 3A): from nucleolus (Ribi), to nucleus (Ribi/RP), to cytosol and plasma membrane (AA); followed by mitochondria (mRP), then large cytosolic structures, such as the endoplasmatic reticulum (ER), proteasomes and lipid droplets (S/C). Thus, the protein products of temporally co-expressed genes also tend to co-localize at their final subcellular destination. Cluster enrichment analysis using the CYC2008 annotation (***Pu et al., 2009***) confirms that many protein complexes are co-expressed during the cycle (Fig. 3D). Large complexes (>10 proteins) involved in basal cellular functions are co-expressed in either HOC or LOC phase, while complexes with regulatory function are comprised of differentially expressed subunits (Fig. S21B).

In a growing cell, fresh ribosomes are constantly built and loaded with the current set of mRNA.

The temporal expression program would lead to spatially structured layers of loaded ribosomes, prior or in parallel to peptide- and mRNA motif-based sorting (***Niessing et al., 2018***), and underpinning co-translational protein complex formation.

## The PWM Model Explains Period Relation to Growth Rate

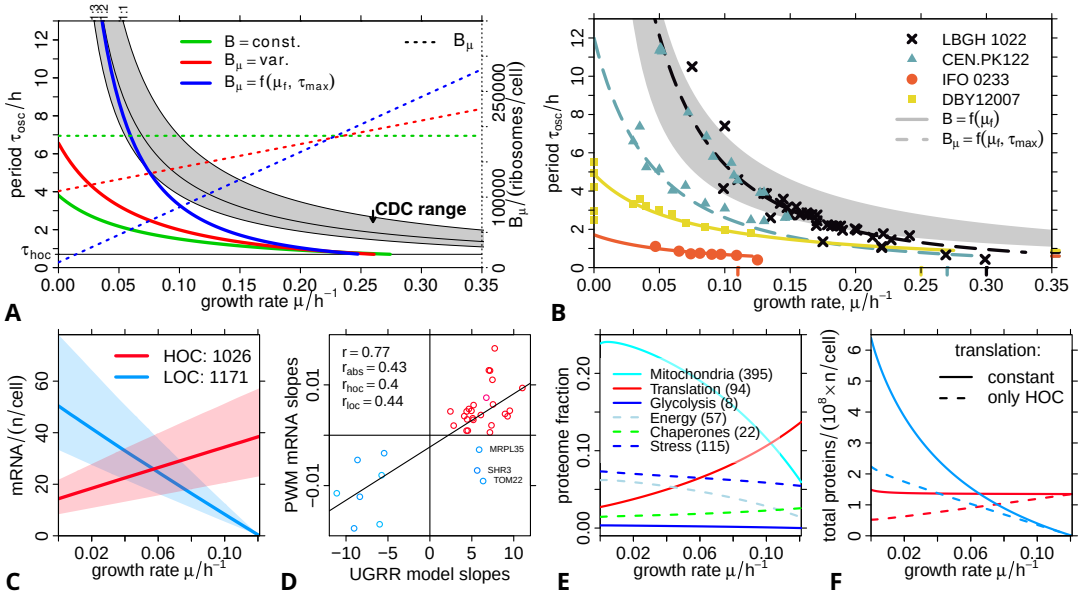


**Figure 4. The Period Growth Rate Relation. A:** Periods predicted by the base model (Eq. 1, solid green line) and the extended model with variable ribosome concentration $B(\mu)$ (Eq. 25, solid red line), with parameters from Table S5. The colored dashed lines are the ribosome concentrations (right y-axis) used for each model. Alternatively, ribosome parameters can be estimated via the $\mu_f$-constraint (Eq. 26, solid blue line). As a reference the periods expected from CDC-synchronization in modes 1:1, 1:2 and 1:3 are shown (black solid lines, Eq. 31-32, (***Bellgardt, 1994***)) and the gray background (CDC range) serves as a reference in all similar plots. **B:** Oscillation periods observed at different growth rates and for different strains (colored points, cf. Fig. S23A) can be reproduced by the PWM model (colored lines) with the same parameters as in (A) but with ribosome concentrations calculated via strain-specific $\mu_f$ (colored ticks on the x-axis) and, for the variable ribosome model (dashed lines), $\tau_{max}$. Additionally $\tau_{hoc}$ (colored ticks on the right y-axis) was manually adjusted (Tab. S6). **C:** Median (lines) and 25%/75% quantiles (transparent range) of all mRNA abundances predicted by the PWM model (Eq. 15) from $\phi_{hoc}$ (IFO 0233 parameters in (B)), and from gene-specific production and degradation rates (Tab. S22B), and classification to either HOC (clusters 1, 2 and 10) or LOC (clusters 6, 7, 8 and 8) phase. The legend indicates the number of genes for which all data was available. **D:** Comparison of the mRNA slopes (C and Fig. S26A) and the slopes provided for signature genes of the UGRR model ***Slavov and Botstein*** (***2011***); data required for PWM-based prediction was available for the shown 35 of 58 signature genes. Gene names are provided for the two outliers. The straight line is a linear regression, and $r$ is the Pearson correlation, $r_{abs}$ removes the influence of the classification by taking the absolute slopes in both data sets, and $r_{hoc}$ and $r_{loc}$ are correlations calculated for only the HOC- or LOC-specific signature genes (red and blue point symbols). **E:** Fractions of the total protein abundance predicted by the PWM model (Eq. 16) for the gene lists used to analyze proteome fractions in ***Metzl-Raz et al.*** (***2017***). Gene numbers in brackets. **F:** Total protein abundances predicted by the PWM model for HOC and LOC phase genes ; calculated without (solid lines, Eq. 16) or with (dashed lines, Eq. 27) an additional restriction of translation to HOC phase. All rates required for mRNA and protein prediction are available in Dataset S3.

Next, we set out to explore the predictive power of the PWM model of gene expression (Appendix B). In short, we assume a step function of transcriptional activity, such that genes are transcribed at maximal rate during their respective expression phase (HOC or LOC) and not transcribed in the other phase (Eq. 15–16). We were intrigued to find that this formulation not only allows to predict mRNA and protein abundances, but yields a strict constraint between oscillation parameters, the life cycle rates and concentration of ribosomes, and growth rate. Ribosomal proteins (RP) are transcribed within the HOC phase clusters (***Klevecz et al., 2004***; ***Machné and Murray, 2012***) (Fig.

3A, D), and assuming that each RP is associated with one ribosome (Appendix B), we get:

$$\frac{\tau_{osc}}{\tau_{hoc}} = \frac{k}{\mu + \delta_r} \frac{\ell}{\mu + \delta_p} \frac{n_B}{B} , \tag{1}$$

where $\tau_{osc}$ and $\tau_{hoc}$ are the oscillation period and the duration of the HOC phase, $\mu$ is the culture growth rate, $B$ is the total concentration of (cytoplasmic) ribosomes, and all other parameters refer to an average RP: $k$ and $\ell$ are transcription and translation rates, $n_B$ is the ribosome density (ribosomes per RP mRNA); and $\delta_r$ and $\delta_p$ are the mRNA and protein degradation rates.

Only $\tau_{loc}$, the time spent in LOC phase (here: $\tau_{loc} = \tau_{osc} - \tau_{hoc}$), reflects changes in growth rate (***Slavov and Botstein, 2011***), while $\tau_{hoc}$ remains constant, or even slightly increased (***Burnetti et al., 2016***), with increasing growth rate. Similarly $\tau_{loc}$ changed consistently with period $\tau_{osc}$, while $\tau_{hoc}$ changed less and in opposite direction during our experiment (Fig. 1B). Thus, we considered a constant $\tau_{hoc}$, and gathered published measurements for all other parameters (Tab. S5, Fig. S22A) to calculate $\tau_{osc}$ at different growth rates. Remarkably, these parameters already yield realistic periods (green line, Fig. 4A) and the non-linear dependence of periods on growth rates (***Bellgardt, 1994***; ***Burnetti et al., 2016***; ***Machné, 2017***). Linearly varying the ribosome concentration with growth rate (Fig. S22C) (***Waldron and Lacroute, 1975***) makes the period function steeper (red line, Fig. 4A).

Periods reach a minimum towards the growth rates $\mu_f$, where yeast metabolism switches from purely respiratory to respiro-fermentative metabolism of glucose (***Burnetti et al., 2016***; ***Machné, 2017***). In IFO 0233, fermentation set in early, at growth rates $\mu_f = 0.11\,\mathrm{h}^{-1}$–$0.15\,\mathrm{h}^{-1}$ (***Hansson and Häggström, 1983***; ***Satroutdinov et al., 1992***) consistent with its short period cycles. This constraint allows to estimate strain-specific specific values for the RP and ribosome-related parameters via published values for $\mu_f$ (Fig. 4B, S23D, Tab. S6). The model with variable ribosomes is required to fit data from the two strains with longer periods (CDC range), or alternatively very low degradation rates (Fig. S23C). This pattern is confirmed when fitting Eq. 1 separately to 20 consistent period data sets (Fig. S24, S25). Long period data sets require to set at least one of the degradation parameters in the denominator to 0. This may be due to a phase-locking with the CDC (***Bellgardt, 1994***) (gray areas in Fig. 4A, B), where the HOC phase aligns with the budding phase of the CDC and LOC phase is purely respiratory (RQ $\approx 1$) and corresponds to the G1 phase of the CDC (***Münch et al., 1992***). When such phase-locking with the CDC occurs, PWM and oscillation parameters may not be directly coupled in this range.

### Qualitative Consistency with Transcriptome and Proteome Data.

Next, we used the fractional HOC phase length ($\phi_{hoc} = \tau_{hoc}/\tau_{osc}$) calculated for IFO 0233 (Fig. 4B), and gene-specific parameters from literature (Fig. S22) to predict mRNA and protein abundances (Eq. 15, 16) for 1,197 genes classified to either HOC or LOC phase clusters (Fig. 4C–F, S26). The Universal Growth Rate Response (UGRR) model allows to predict growth rate based on the relative mRNA abundances of 58 signature genes selected by a strong negative or positive correlation of mRNA abundances with growth rate (***Airoldi et al., 2009***; ***Slavov and Botstein, 2011***). The mRNA abundance slopes calculated from the PWM prediction (Fig. 4C) correlated well with the growth rate-dependent slopes of the UGRR model's signature genes (Fig. 4D). Similarly, we found good overall agreement of the relative proteome fractions at different growth rates of gene groups selected by ***Metzl-Raz et al.*** (***2017***) (Fig. 4E). For example, the proteome fraction of mitochondrial genes decreases, while the fraction of genes involved with translation increase with growth rate, reflecting measurements (***Paulo et al., 2016***; ***Metzl-Raz et al., 2017***).

### Quantitative Discrepancies Explained by Chromatin Structure and Energetic Constraints.

However, quantitively our predictions are off for some gene groups. For example the "translation" gene group occupies only 3% to 14% of the proteome in the PWM prediction, while this ranged from 19% to 38% in the proteome data evaluated by ***Metzl-Raz et al.*** (***2017***). In contrast, proteins from the "stress" group are overestimated ≈2x by the PWM prediction. Total mRNA abundances are within the range of published estimates (***Hereford and Rosbash, 1977***; ***Zenklusen et al., 2008***) at high

growth rates, but 1.5x too high at low growth rates (Fig. S26B). Total protein abundances are within the estimated range (***Milo, 2013***) only at the highest growth rate, and 6x fold too high at slow growth (Fig. 4F, S26F). When comparing all gene-wise predictions with data, the main contribution for the good overall correlation stems from correct classification into HOC phase or LOC phase-specific genes, while correlations are low, absent or even negative within the two groups (Fig. S26C,G). This only slightly improves when focusing on the subsets of genes in a previously defined consensus clustering (***Machné and Murray, 2012***) of co-expression cohorts (Fig. S26D,H).

These errors help to pinpoint weaknesses of the model, and suggest directions for future extensions. The `Ribi` and `RP` cohorts (HOC) are characterized by large nucleosome-free regions (NFR) in their promoter, while the `S/C` (LOC) cohorts have occupied promoters and a less defined gene body nucleosome structure (***Lee et al., 2007***; ***Machné and Murray, 2012***). Total nucleosome occupancy (histone H3) at transcription start sites was lower in HOC and reached a maximum in LOC phase, anti-phase to histone acetylation (H3K9ac) and RNA polymerase II binding (***Amariei et al., 2014***). Nucleosomes act as a barrier to RNA polymerase (***Jimeno-González et al., 2015***), and different chromatin structures are accompanied by different modes of transcription (***Kristjuhan and Svejstrup, 2004***; ***Zenklusen et al., 2008***). These observations all suggest that transcription of LOC phase-associated genes occurs at lower overall rates, which would rectify some of the observed discrepancies between model and data.

Similarly, translation rates could differ between the co-expression cohorts; e.g. RP genes are often assumed to have optimized codon usage, contributing to high RP abundances (***Jansen et al., 2003***). However, we believe a more significant over-simplification of the model leads to the overestimation of protein abundances at low growth rates. Protein biosynthesis is globally regulated by nutrient availability via the TOR1 kinase. Its inhibitor rapamycin immediately stops HOC phase and induces a long phase of low respiratory activity in both IFO 0233 and CDC-coupled systems (***Murray et al., 2007***; ***O' Neill et al., 2020***). Cumulative evidence suggests (Appendix B.5) that a TOR1-mediated translational pulse occurs during HOC phase or at the transition from HOC to LOC phase, when the ATP/ADP ratio is high and then rapidly drops. As a first approximation of this phenomenon, we additionally assumed that translation of all transcripts occurs exclusively in HOC. Indeed, this assumption (Eq. 27) leads to more realistic total protein abundances at low growth rates (dashed lines in Fig. 4F, S26F,J). However, when using this assumption in period estimation, the obtained results are confined to short periods (Fig. S26K). Future work based on this novel theoretical framework should explicitly account for energetic constraints (Fig. 1) on the protein synthesis capacity during the cycle.

## Discussion

The phenomenon of metabolic auto-synchronization in budding yeast continuous culture was instrumental for the clarification of the asymmetric CDC of budding yeast (***Küenzi and Fiechter, 1969***; ***von Meyenburg, 1969a***). The discovery of stable short period cycles in the distillery strain IFO 0233 (***Satroutdinov et al., 1992***) fortified early indications (***von Meyenburg, 1969b***; ***Mochan and Pye, 1973***) that the system is more than just synchronization of the CDC. Here, we first explored the complexity of dynamics observable in budding yeast continuous culture, a long-term transient and a sudden bifurcation, then tested the two main hypotheses on putative functions of the periodic transcriptome (**H1** and **H2**), and developed a novel model (**H3**).

Filtering for short-lived proteins with high mRNA amplitude again highlights previously suggested candidate pathways (***Keulers et al., 1996***; ***Murray et al., 1999***, ***2003***, ***2007***) that may play a role in the control of metabolic dynamics and population synchronization (**H1**). These pathways also show distinct flux changes during the observed bifurcation of system dynamics; specifically $H_2S$, the gaseous intermediate of sulfate uptake and an inhibitor of the $O_2$-reaction in respiration; and perhaps more intriguingly, the prime waste product of heterotrophic organisms, $CO_2$. ***Aguilera et al.*** (***2005***) found that $HCO_3^-$ can be a limiting anabolic substrate in aerated liquid cultures and colonies in the absence of carbonic anhydrase (NCE103). A sulfate uptake transporter (SUL1) and

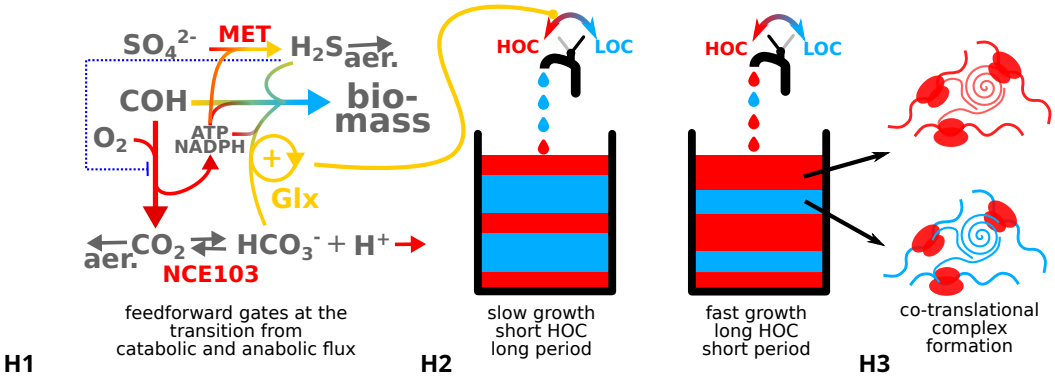


**Figure 5. Summary Cartoon Models. H1, Just-in-time Expression:** Putative interactions between catabolic and anabolic flux during the cycle. Sulfate uptake (MET), $CO_2$ sequestration (NCE103) and the glyoxylate cycle (Glx) all involve short-lived proteins with high mRNA abundance amplitude, peaking with the `Ribi` and `AA` cohorts, and require ATP and NADPH from catabolism of carbon sources (COH), forming a multi-branch feedforward gate that can kick-start the biosynthetic pulse at the transition from the HOC to the LOC phase. Colors indicate approximate phase relations (red: HOC, yellow: transition:, blue: LOC; more details in Fig. S19) . **H2, Pulse-Width Modulation:** Pulse-width modulation (PWM) of expression phases may adapt protein abundances to different growth conditions, here visualized as a water-tap switching between supply of HOC and LOC phase-specific liquid (transcripts). **H3, Protein Homeostasis:** The temporal transcription program could underpin spatial assembly of translating ribosomes and co-translational complex formation.

---

NCE103 were also among the top oscillators in a recent proteomic study of a long period system (***O' Neill et al., 2020***). Potential roles of the periodic abundances of enzymes of these pathways and of the auto-catalytic glyoxylate cycle (***Barenholz et al., 2017***), e.g. in a multi-branched feedforward gate between catabolic and anabolic phases of the cycle (H1 in Fig. 5), are promising candidates for further research into the mechanistics of metabolic dynamics. In Figure S19 we provide an integrative picture, and the Datatable S1 can be used to test these speculative scenarios.

Consistent with our estimation, the majority of protein abundances did not oscillate in long period systems (***O' Neill et al., 2020***; ***Feltham et al., 2019***). ***Slavov and Botstein*** (***2011***) suggested that periodic transcript abundances could serve to balance steady-state protein abundances with growth rate by differential variation of the length of the expression phases (**H2** in Fig. 5). When translating this idea to a mathematical model, parameterized with published data, we find that it can indeed account for the relation of growth rate to the ribosomal biomass fraction (***Schaechter et al., 1958***; ***Molenaar et al., 2009***; ***Scott et al., 2010***), and to the relative abundances of large, functionally coherent classes of transcripts and proteins (***Brauer et al., 2005***; ***Paulo et al., 2016***; ***Metzl-Raz et al., 2017***). Furthermore, the PWM model can also explain the relation of cycle periods to growth rate. This is the first mechanistic model for this relation since the CDC-based population synchrony models (***Bellgardt, 1994***; ***Hjortso and Nielsen, 1995***; ***Duboc and von Stockar, 2000***), but can also account for short periods and oscillations without cell division (***Mochan and Pye, 1973***; ***Murray, 2004***; ***Slavov et al., 2011***). It provides a novel theoretical framework to study this phenomenon, essentially as a mechanism of cellular resource allocation. The same problem exists in diurnal context, where only few protein abundances oscillate (***Lück et al., 2014***; ***Wang et al., 2018***; ***Krahmer et al., 2021***; ***Karlsen et al., 2021***). The $24\,\mathrm{h}$ period is constant, but seasonal changes in light/dark phase lengths could mediate PWM-based control of steady state protein abundances.

We found that a significant change in expression peak widths can occur within two cycles. This was not reflected in metabolic rates, that is, transcription is not just an output of metabolism (**H0**, ***Feltham et al.*** (***2019***)). This change was, however, directly followed by a pronounced bifurcation of metabolic dynamics. This exemplifies that the hypotheses tested here are not mutually exlusive. Peak width modulation (**H2**) can occur fast, and could have direct consequences on metabolic dynamics via short-lived proteins (**H1**).

### Outlook.

***Slavov et al.*** (***2012***) suggested the existence of a conserved eukaryotic cell growth cycle which, at slow growth, can be traversed multiple times during the biomass accumulation phases (G1 or G2) of the CDC. Nitrogen uptake (***von Meyenburg, 1969b***), and amino acid (***Hans et al., 2003***) and protein biosynthesis (***O' Neill et al., 2020***) were associated with HOC phase or with transition to LOC phase (***Murray et al., 2007***). This coincides with the G1/S transition in dividing cells (***Münch et al., 1992***; ***Klevecz et al., 2004***). Pulses of biomass growth or protein production were directly observable in single cell studies at the G1/S transition (***Cookson et al., 2010***; ***Bryan et al., 2010***; ***Litsios et al., 2019***), and multiple pulses per CDC were observed in mammalian cells (***Liu et al., 2020***; ***Ghenim et al., 2021***). Here, we further suggest that these translational bursts act on spatially pre-organized layers of mRNA:ribosome complexes (**H3** in Fig. 5), facilitating co-translational protein folding and complex formation (***Shiber et al., 2018***; ***Schwarz and Beck, 2019***) and spatial sorting of the proteome. Such a spatial pre-sorting could be generated by the temporal sequence of transcript synthesis and loading of fresh ribosomes in the growing cell – a reaction-diffusion mechanism (***Turing, 1952***) for subcellular pattern formation. In LOC phase, increased protein aggregation (***O' Neill et al., 2020***) at low ATP/ADP ratios (***Amariei et al., 2014***; ***Xu et al., 2004***) and low pH (***Keulers et al., 1996***; ***O' Neill et al., 2020***) could then serve to remove misfolded or otherwise damaged protein complexes. Knock-out or mutation of the prion-like (Q/N-rich) protein Gts1p (***Sanada et al., 2011***; ***Ripaud et al., 2014***) affected oscillations in all period ranges (***Wang et al., 1998***; ***Adams et al., 2003***; ***Liu et al., 2002***; ***Saito et al., 2002***). This perspective, a function of the cycle in protein homeostasis (***O' Neill et al., 2020***) and spatial organization, may also provide a framework to understand our observation that non-coding RNA transcript abundances peaked in LOC phase, where they could help to organize membrane-less compartmentation (***Maharana et al., 2018***; ***Quinodoz et al., 2021***). We speculate that, at low cellular energy, LOC phase may be a phase of assembly, clean-up and spatial self-organization of the growing cell.

## Supporting Information and Data

### Supporting Information File:

Appendices A, B and all Supporting Figures.

### Dataset S1:

Reactor data, including all calculated rates and RNA-seq samples IDs.

### Dataset S2:

All 36,928 segments reported by `segmenTier`, incl. genome coordinates, cluster labels, read-counts, oscillation values (amplitude $A_2$, phase $\phi_2$, p-value $p_{\text{rain}}$), coding gene and SUT overlaps, and all time points, using the sampling IDs (2–25) indicated in the reactor data.

### Dataset S3:

Data for 3,849 coding genes that overlap with a segment with $J > 0$: relative mRNA and protein amplitudes and protein half-lives for prediction of protein amplitudes (Fig. S17), and production and degradation rates as used for period, mRNA and protein abundance predictions, incl. cluster associations and classification as RP gene (Fig. S22A/B, Tab. S5).

## Materials and Methods

### Strain History

Kuriyama's lab first reported oscillations in continuous culture of the *Saccharomyces cerevisiae* strain IFO 0233 (***Satroutdinov et al., 1992***). The strain number is from the Japanese culture collection NBRC and is identified there as "`Distillery yeast Rasse II`", "accepted" in 1941, and as ATCC 560 in the US American culture collection. These strains can be traced back to the "Brennereihefe, Rasse II" isolated as "Hefe 128" axenic culture by Paul Lindner at the Berlin Institut für

Gärungsgewerbe in 1889 from samples of a distillery in Gronowo (West Prussia, now Poland) which obtained their yeast from a dry yeast supplier in the city Thorn (now Toruń, Poland) (***Lindner, 1895***). The strain and its descendant "Rasse XII" became commercially successful distillery strains within hybrid formulations ("Rasse M"), and was at the time an intensively studied strain in basic research, *e.g.*, in the search for the nature of "bios" (***Lindner, 1919***).

## Continuous Culture

### Pre-Culture

*Saccharomyces cerevisiae* (strain IFO 0233) were maintained on yeast nitrogen base agar plates ($2\,\%$ glucose, $1.5\,\%$ agar; Difco, Japan) at $4\,°\mathrm{C}$, sub-cultured from frozen stock cultures (-$80\,°\mathrm{C}$; $1\,\mathrm{mL}$; $15\,\%$ glycerol; $5 \times 10^8$ cells). Pre-cultures were inoculated into Yeast Extract Peptone Dextrose media ($10\,\mathrm{mL}$; $1\,\%$ yeast extract, $2\,\%$ peptone, $2\,\%$ glucose) and grown at $30\,°\mathrm{C}$ in an orbital incubator ($200\,\mathrm{rpm}$) for $24\,\mathrm{h}$.

### Continuous Culture Medium & Inoculation

The culture medium consisted of D-glucose ($20\,\mathrm{g\,L^{-1}}$), (NH4)2SO4 ($5\,\mathrm{g\,L^{-1}}$), KH2PO4 ($2\,\mathrm{g\,L^{-1}}$), MgSO4.7H2O ($0.5\,\mathrm{g\,L^{-1}}$), CaCl2.2H2O ($0.1\,\mathrm{g\,L^{-1}}$), FeSO4.7H2O ($20\,\mathrm{mg\,L^{-1}}$), ZnSO4.7H2O ($10\,\mathrm{mg\,L^{-1}}$), CuSO4.5H2O ($5\,\mathrm{mg\,L^{-1}}$), MnCl2.4H2O ($1\,\mathrm{mg\,L^{-1}}$), $70\,\%$ H2SO4, ($1\,\mathrm{mL\,L^{-1}}$), Difco yeast extract ($1\,\mathrm{g\,L^{-1}}$) and Sigma Antifoam A ($0.2\,\mathrm{mL\,L^{-1}}$). All chemicals were supplied by Wako Pure Chemical Industries Ltd., Japan. The medium prepared with this recipe has a pH of ca. 2.5 which allows for autoclaving of media with both sugar and ammonium without browning (caramelization) and further avoids precipitation of salts in feed medium bottles during continuous culture. A custom-built bioreactor as outlined below was filled with $0.635\,\mathrm{L}$ of medium and autoclaved ($121\,°\mathrm{C}$; $15\,\mathrm{min}$). Aeration ($0.15\,\mathrm{L\,min^{-1}}$), agitation ($750\,\mathrm{rpm}$), and temperature ($30\,°\mathrm{C}$) and pH (3.4) control were switched on, until the system was equilibrated. Then, the dissolved oxygen probe was 2-point calibrated by flushing with pure nitrogen ($0\,\%$) and switching back to air ($100\,\%$). The equilibrated and fully calibrated reactor was inoculated with $\approx 1 \times 10^9$ pre-culture yeast cells. A batch phase continued for $\approx 40\,\mathrm{h}$ until the cells had reached stationary phase, indicated by a sharp decrease in respiratory activity. Then continuous culture, *i.e.*, feeding with fresh medium, was initiated (at $44.5\,\mathrm{h}$ in Figure 1).

### Culture Control & Monitoring

Continuous culture was performed in a custom-built bioreactor. The culture vessel was a jar fermentor (Eyela, Japan) with a total volume of $2.667\,\mathrm{L}$. Culture volume was measured using a balance (SB16001, Mettler Toledo, Japan), and continuous dilution with fresh medium was performed using a peristaltic pump (AC2110, ATTA, Japan) with a six roller planetary design which minimizes pulsing during rotation (about $10\,\mathrm{rpm}$), and medium was pumped through $1\,\mathrm{mm}$ tubing (inner diameter; Masterflex, Cole Palmer, USA) and a 23 gauge steel needle. This ensured that the media was introduced in a stream of $<20\,\mu\mathrm{L}$ droplets and just under a droplet per second at the operating dilution rate. Feed medium bottle weight was monitored by a balance (PMK-16, Mettler Toledo, Japan), set up to read from unstable environments and shielded from direct breezes. The culture was agitated at $750\,\mathrm{rpm}$ and aerated at $0.150\,\mathrm{L\,min^{-1}}$ by a mass flow controller (B.E. Marubishi, Japan). Dissolved oxygen was measured using an InPro 6800 sensor and pH with an InPro 3030 (both: Mettler Toledo, Japan). Culture pH was maintained at 3.4 by the automatic addition of $2.5\,\mathrm{mol\,L^{-1}}$ NaOH, and the weight of the NaOH bottle was monitored on a balance (PM400). Local control of agitation and pH was carried out by Labo controllers (B.E. Marubishi, Japan). The reactor pressure was monitored by a manometer (DM-760, Comfix, Japan) installed on a split outlet flow stream. The culture temperature was controlled at $30\,°\mathrm{C}$ by an external sensor connected to a circulating water bath (F25-ME, Julabo, Japan). Partial pressure of oxygen and carbon dioxide in the off-gas were measured by an Enoki-III gas analyzer (Figaro engineering, Japan). The partial pressure of hydrogen sulfide in the off-gas was measured using an electrode based gas monitor (HSC-1050HL, GASTEC, Japan). Instruments were calibrated as per manufacturer's instruction.

### Reactor Data Acquisition and Calculation of Metabolic Rates

Data were acquired *via* the in-house `FERMtastic` software at 0.1 Hz. Metabolic rates were calculated as described previously (***von Meyenburg, 1969a***; ***Heinzle, 1987***; ***Verduyn et al., 1991***; ***Marison et al., 1998***; ***Murray et al., 2007***) from the online recorded data. Details and all equations are provided in Appendix A of the supporting information. All data were processed in the script `samplingSeq_2019.R` of the `yeastSeq2016` git repository. All calculated rates are provided in Dataset S1.

## RNA Sequencing & Read Mapping

### Sampling, RNA Extraction & Sequencing Library Generation

Total RNA was extracted as previously described (***Sasidharan et al., 2012***) from 24 samples taken every 4 min, covering ca. 2.5 cycles of the respiratory oscillation.

Culture samples were immediately quenched in ethanol and disrupted using acid-washed zirconia/silica beads (0.5 mm; Tomy Seiko Co., Ltd., Japan) with sodium acetate buffer (250 µL; sodium acetate 300 mM, Na2-EDTA 10 mM , pH 4.5–5.0) and one volume of TE-saturated phenol (Nacalai Tesque) equilibrated with sodium acetate buffer (250 µL).

The samples were then centrifuged (12 000 g, 15 min, 4 °C) and the aqueous phase transferred to fresh 1.5 mL microcentrifuge tubes. Back-extraction was performed by adding sodium acetate buffer (125 µL) to the bead-beat tubes, vortex (10 s), centrifuging (12 000 g, 15 min, 4 °C) and adding the aqueous phase to the first aqueous phase. 2.5 volumes ice-cold 99.5 % ethanol were added to the aqueous phase and RNA/DNA precipitated at −20 °C overnight. The samples were then centrifuged (12 000 g, 30 min, 4 °C), the supernatant removed by aspiration, and pellets washed 3× in 500 µL 70 % ethanol and air-dried (10 min, room temperature). DNA was removed (RNase-Free DNase Set; Qiagen, Japan) and RNA recovered by column purification (QIAquick PCR Purification Kit; Qiagen, Japan) in 50 µL UltraPure water, and stored at −80 °C prior to analysis. Total RNA had an RNA integrity number >7 and 260nm:230nm and 260nm:230nm ratios >2.14. All cDNA libraries were then generated and sequenced by the Beijing Genome Institute (BGI), China. Strand specific cDNA libraries were created using the "dUTP method" (***Parkhomchuk et al., 2009***; ***Levin et al., 2010***) and sequencing was carried out on an Illumina 1G sequencer.

### RNA-seq Read Mapping

RNA-seq reads were mapped against the yeast reference genome (strain S288C, release R64-1-1) using `segemehl` (version 0.1.4) (***Hoffmann et al., 2014***) with default parameters and spliced read mapping enabled. Initially unmatched reads were mapped again using the remapping tool from the `segemehl` package and the resulting files were merged. Coverage (read-counts per nucleotide) was normalized for total library size to reads-per-million (RPM) and RPM values were stored in a bedgraph file for further analysis.

## RNA-seq Time Series Analysis

### Analysis Strategy and R Packages

All analyses were performed with bash and R. The full analysis pipeline is available in a git repository at https://gitlab.com/raim/yeastSeq2016. Analysis and plotting tools developed for this work are available in an git repository with scripts and an R package available at https://github.com/raim/segmenTools. RNA-seq segmentation was performed with the `segmenTier` R package (***Machné et al., 2017***), available at https://cran.r-project.org/package=segmenTier. Scripts for genome-wide data collections and mapping to the yeast S288C reference genome (release R64-1-1) as well as the `genomeBrowser` plots are available at the git repository https://gitlab.com/raim/genomeBrowser.

### Additional Data Sources

Genome annotations including Gene Ontology (GO) terms were taken directly from the gff genome file from the *Saccharomyces* genome database (SGD, release R64-1-1, 2011-02-08, same as for RNA-

seq mapping). Published transcript data sets (XUT, SUT, etc.) were also obtained from SGD for the same genome release. Protein complex annotation CYC2008 (***Pu et al., 2009***) was downloaded from http://wodaklab.org/cyc2008/resources/CYC2008_complex.tab on 2019-06-04. Published period and growth rate-related data were obtained from https://gitlab.com/raim/ChemostatData, a data collection for ***Machné*** (***2017***), which also contains R scripts for analysis, incl. period models described in Appendix B. All other data were obtained from the supporting material of publications: half-live data for mRNAs and proteins from ***Geisberg et al.*** (***2014***) and ***Christiano et al.*** (***2014***); ribosome density data from ***Arava et al.*** (***2003***); the consensus clustering of periodically expressed transcripts from ***Machné and Murray*** (***2012***); UGRR expression data and slopes from ***Slavov and Botstein*** (***2011***); protein abundance data from ***Paulo et al.*** (***2016***), where growth rate data was sent in personal communication; and functional gene groups from (***Metzl-Raz et al., 2017***).

## Discrete Fourier Transform.

A time series of $N$ measurements $x = \{x_0, \dots, x_{N-1}\}$, taken at equally spaced time points $\{t_0, \dots, t_{N-1}\}$, can be transformed to frequency-space by the Discrete Fourier Transform (DFT):

$$X_k = \sum_{n=0}^{N-1} x_n e^{-2\pi i \frac{kn}{N}} \quad , \quad k = \{0, \dots, N-1\} \tag{2}$$

where $X_k$ is a vector of complex numbers representing the decomposition of the original time series into a constant (mean) component (at $k = 0$) and a series of harmonic oscillations around this mean with periods $P_k$, amplitudes $A_k$ and phase angles $\phi_k$:

$$\begin{aligned} P_k &= (t_{N-1} - t_0)/k \,, \\ A_k &= |X_k|/N \,, \\ \phi_k &= -\text{atan2}(\text{Im}(X_k), \text{Re}(X_k)) \,. \end{aligned} \tag{3}$$

All DFT were performed with R's `fft` function.

For DFT-based clustering and segmentation analysis, it proved useful to scale DFT components by the mean amplitude of all other components $k > 0$:

$$X'_{k>0} = \frac{X_{k>0}}{\overline{|X|}_{k \neq \{0,k\}}} \,, \tag{4}$$

and the constant component ($k = 0$) by the `arcsinh` transformation:

$$X'_0 = \ln\left(|X_0| + \sqrt{X_0^2 + 1}\right) . \tag{5}$$

For analysis of read-count data $x_n$ were the raw read-counts, for analysis of segments $x_n$ were the mean of all read-counts of the segment.

The index $k$ corresponds to the number of full cycles with period $P_k$ in the time series. Only the first 19 time points, covering two full cycles of the oscillation were used for the calculation of phases and p-values, such that $k = 2$ reflects the main oscillation. For all plots, phases were shifted such that $\phi_2 = 0$ corresponds to the transition from LOC to HOC.

## Oscillation p-Values

For calculation of oscillation p-values $p_{\text{DFT}}$ on read-count level the time series were permutated $N_p = 10,000$ times, and random amplitude $\tilde{A}_2$ calculated. The p-value was estimated as the fraction of permutations for which the random amplitude was larger than the observed amplitude $A_2$ (eqn. 3). This analysis was performed with the script `genomeOscillation.R` from the `segmenTools` git repository. Oscillation p-values $p_{\text{rain}}$ on segment level were calculated with the R package `rain` (***Thaben and Westermark, 2014***) using period $P = 0.65\,\text{h}$ and time step $\delta t = 4\,\text{min}$. This analysis was done with the script `segmentDynamics.R` from the `segmenTools` git repository.

## Segmentation of RNA-seq Read-Counts & Segment Classification

The data were pre-segmented into expressed and weakly expressed chromosomal domains by a previously described heuristic (***Machné et al., 2017***) with a minor correction that splits pre-segments at chromosome ends. Pre-segmentation was done with the script `presegment.R` from the `segmenTools` script collection; Figure S7 provides pre-segment length distributions and run parameters. Pre-segments were then individually split into non-overlapping segments with coherent temporal expression profiles by the `segmenTier` algorithm, using optimized parameters from our previous study (***Machné et al., 2017***). Shortly, the `arcsinh`-transformed read-count data was Fourier-transformed (Eq. 2); the first component ($k = 0$), reflecting the mean expression level, was `arcsinh`-transformed (Eq. 5); and all other ($k > 0$) components were amplitude-scaled (Eq. 4). The real and imaginary parts of the scaled DFT components $X'_{k=0,\ldots,6}$ were then clustered into 12 groups with R's implementation of `k-means` (using the `Hartigan-Wong` method or if that failed, the `MacQueen` method). This clustering then provided the anchors for the similarity-based segmentation by the `segmenTier`, where we used the `icor` scoring function with exponent $\epsilon = 2$, length penalty $M = 150$, nuissance cluster penalty $M_0 = 100$, and nuissance cluster exponent $\nu = 3$. This combination of parameters is achieved by arguments `-trafo "ash" -dc.trafo "ash" -dft.range 1,2,3,4,5,6,7 -K 12 -Mn 100 -scores "icor" -scales 2 -M 150 -nui.cr 3` to the `runSegmentier.R` script in the `segmenTools/scripts` collection. All segments are provided in Dataset S2.

The resulting segments were then filtered and classified by their oscillation p-values ($p_{\text{rain}}$, see above) and their overlaps with transcribed features annotated in the reference genome (release R64-1-1), using `segmentOverlaps.R` and `segmentAnnotation.R` in the `segmenTools/scripts` collection. Overlaps were quantified as the Jaccard index, $J = \frac{I}{U}$, where $I$ is the intersect, the number of overlapping nucleotides, and $U$ the union, the number of nucleotides covered by both, the segment and the annotated feature. Table S2 provides details on filtering and the resulting sizes (numbers) of analyzed segment sets. Figure S8 provides the full data structure which guided these threshold choices.

## Segment Clustering

The means of read-counts covered by a segment were taken as segment time series. Periodic expression was analyzed by permutation analysis and DFT and by the R package `rain`. 11,248 segments with $p_{\text{rain}} < 0.85$ were chosen for further analysis (Fig. S8E-F). The DFT of the segment time series was amplitude-scaled (Eq. 4, Fig. S9A) and the first (constant) component ($k = 0$) was `arcsinh`-transformed (Eq. 5). Real and imaginary parts of the scaled DFT components $X'_{k=0,\ldots,6}$ were then clustered with the `flowClust` algorithm (***Lo et al., 2009***) for cluster numbers $K = 2, \ldots, 16$. The clustering with the maximal Bayesian Information Criterion, as reported by `flowClust` (Fig. S9B), was selected for further analysis. Clustering was performed by `clusterTimeseries2` function of `segmenTools` *via* the `segmentDynamics.R` script). The resulting clustering was sorted, re-labeled and colored automatically based on the means of their segments' expression phases (Eq. 3). The clustering was further sub-divided into high-amplitude clusters enriched for coding genes and low-amplitude clusters (compare Fig. S10 and S11).

## Relative Protein Amplitudes

3,189 segments overlapping with a coding region with Jaccard index $J > 0.5$ and with protein half-live ($\tau_{1/2}$) annotation in (***Christiano et al., 2014***) were considered. Proteins with half-life annotation ">=100" were treated as $\tau_{1/2} = \infty$. The relative mRNA amplitudes were calculated from the DFT $X_k$ (Eq. 2-3) of the first 19 time points (2 full cycles) of the RNA-seq read count time series as $A_{\text{mRNA}} = X_2/X_0$, *i.e.*, the ratio of the amplitudes of the $2^{nd}$ component $X_2$ (2 cycles) over the $0^{th}$ component $X_0$ (corresponds to the mean over all time points) of the DFT. Relative protein amplitudes $A_{\text{protein}}$ were then calculated with the analytical solution to an ordinary differential equation of rhythmic production, after equation S8 of (***Lück et al., 2014***), as

$$A_{\text{protein}} = A_{\text{mRNA}} \frac{\gamma}{\sqrt{\gamma^2 + \omega^2}}\,, \tag{6}$$

with angular frequency $\omega = \frac{2\pi}{\tau_{osc}}$ and $\tau_{osc} = 0.67\,\text{h}$; the total protein degradation rate $\gamma = \delta_p + \mu$, where the actual protein degradation rates $\delta_p$ were taken from (***Christiano et al., 2014***); and the growth rate equals the chemostat dilution rate $\mu = \phi = 0.089\,\text{h}^{-1}$. In this model, the relative amplitude $A_{\text{mRNA}}$ is assumed to directly reflect periodic production,*i.e.*, translational activity. Total amounts or translation rates are not required, and only a relative amplitude of protein amount can be calculated. Predicted protein amplitudes are provided in Dataset S3.

### Peak Width Analysis

For each high-amplitude segment (2,505 segments with $p_{\text{rain}} < 0.0001$) the time series was interpolated to 1° resolution ($0.105\,\text{min}$), and the oscillation phase $\phi_2$ (Eq. 3) was used as anchors to scan for times spent above the temporal median $\tilde{x}$ during the first and the second full cycle in the data set (horizontal arrows in Fig. 2A). These times were recorded as the peak widths $W_1$ and $W_2$. The peak width change is the difference $\Delta W = W_2 - W_1$. Only segments with peak phases with ≥60° distance to the start or end of the timeseries and where the median expression was traversed twice within one cycle were considered, resulting in 2,357 segments with $\Delta W$ values. $\Delta\Delta W$ was calculated as the difference of the medians of $\Delta W$ of the two extreme segment clusters 1 and 8.

## Cluster Enrichment Analyses

### Cluster-Cluster Enrichment Tests

Categorical enrichments, *e.g.* coding gene co-expression cohorts *vs.* gene annotations, were analyzed by cumulative hypergeometric distribution tests (R's `phyper`) using `segmenTools`'s `clusterCluster` function and the `clusterAnnotation` wrapper for GO and and protein complex analysis, which compares overlaps of each pair of two distinct classifications into multiple classes, and stores overlap counts and p-values ("enrichment tables") for informative plots (see "Enrichment Profiles").

In these tests, the complete set of ORF annotated in the reference genome was analyzed (urn size: 5,795). Of these, 4,489 ORF that overlapped with an segment (Tab. S2) with a Jaccard index $J > 0.5$ were assigned to this segment's cluster, where non-clustered segments ($p_{\text{rain}} \geq 0.85$) were assigned to cluster "0", and all non-overlapping ORF ($J_{\text{ORF,max}} < 0.5$) assigned to the "n.a" cluster. For the analysis of protein complex analysis, all 5,524 ORF that overlapped with a segment with $J_{\text{ORF}} > 0$, and the one with the maximal $J_{\text{ORF}}$ was used for cluster assignment. This relaxed assignment was used to comprehensively capture complex co-expression and differential expression.

### Enrichment Profiles

The results of multi-class enrichment tests (segment overlaps or cluster-cluster categorical overlaps) were visualized as colored table plots, *e.g.* Figure 3A), using `segmenTools`' function `plotOverlaps`. The total counts of overlapping pairs are plotted as text, where the text color is selected based on a p-value cutoff $p_{\text{txt}}$ (as indicated). The background color gray level of each field scales with $\log_2(p)$, such that fields with a minimal p-value $p_{\text{min}}$ (as indicated) are black.

For intuitively informative plots the enrichment tables were sorted. Table rows were sorted along the other dimension (table columns) such that all categories enriched above a certain threshold $p_{\text{sort}}$ in the first column cluster are moved to the top, and, within, sorted by increasing p-values. Next, the same sorting is applied to all remaining row clusters for the second column cluster, and so on until the last column cluster. Remaining row clusters are either plotted unsorted below a red line or removed. This is especially useful to visualize enrichment of functional categories along the temporal program of co-expression cohorts, *e.g.*, Figure 3A and D. This sorting is implemented in `segmenTools`' function `sortOverlaps`.

## Author Contributions

DBM designed and performed the experiment, SHB performed the RNA-seq read mapping, RM and PFS developed the segmentation algorithm. RM and IMA analyzed the time series data. All authors contributed to data interpretation and to writing of the manuscript.

## Acknowledgments

We thank Sarah Lück, Oliver Ebenhöh, Wolfram Liebermeister, Ovidiu Popa, Chilperic Armel Foko Kuate and St. Elmo Wilken for inspiring discussions of the data and critical review of the manuscript. We are grateful to Martin Senz from the Berliner Institut f. Gärungsgewerbe und Biotechnologie, a successor of Paul Lindner, for help with clarifying the origin of the IFO 0233 strain.

## Funding

DBM was funded by a partnering award from Japan Science and Technology Agency, Yamagata prefectural government and the City of Tsuruoka. RM was funded by the *Deutsche Forschungsgemeinschaft*, grants AX 84/4-1 and STA 850/30-1. IMA and RM were funded by EXC-2048/1–project ID 390686111 (CEPLAS).

## References

**Adams CA**, Kuriyama H, Lloyd D, Murray DB. The Gts1 protein stabilizes the autonomous oscillator in yeast. Yeast. 2003 Apr; 20(6):463–470. doi: 10.1002/yea.976.

**Aguilera J**, Van Dijken JP, De Winde JH, Pronk JT. Carbonic anhydrase (Nce103p): an essential biosynthetic enzyme for growth of *Saccharomyces cerevisiae* at atmospheric carbon dioxide pressure. Biochem J. 2005 Oct; 391(Pt 2):311–316.

**Airoldi EM**, Huttenhower C, Gresham D, Lu C, Caudy AA, Dunham MJ, Broach JR, Botstein D, Troyanskaya OG. Predicting cellular growth from gene expression signatures. PLoS Comput Biol. 2009 Jan; 5(1):e1000257. doi: 10.1371/journal.pcbi.1000257.

**Amariei C**, Machné R, Stolc V, Soga T, Tomita M, Murray DB. Time resolved DNA occupancy dynamics during the respiratory oscillation uncover a global reset point in the yeast growth program. Microb Cell. 2014 Sep; 1(9):279–288. doi: 10.15698/mic2014.09.166.

**Aon MA**, Roussel MR, Cortassa S, O'Rourke B, Murray DB, Beckmann M, Lloyd D. The scale-free dynamics of eukaryotic cells. PLoS One. 2008; 3(11):e3624. doi: 10.1371/journal.pone.0003624.

**Arava Y**, Wang Y, Storey JD, Liu CL, Brown PO, Herschlag D. Genome-wide analysis of mRNA translation profiles in Saccharomyces cerevisiae. Proceedings of the National Academy of Sciences. 2003; 100(7):3889–3894. https://www.pnas.org/content/100/7/3889, doi: 10.1073/pnas.0635171100.

**Barenholz U**, Davidi D, Reznik E, Bar-On Y, Antonovsky N, Noor E, Milo R. Design principles of autocatalytic cycles constrain enzyme kinetics and force low substrate saturation at flux branch points. Elife. 2017 Feb; 6. doi: 10.7554/eLife.20667.

**Bellgardt KH**. Analysis of synchronous growth of baker's yeast. Part I: Development of a theoretical model for sustained oscillations. Journal of Biotechnology. 1994; 35(1):19 – 33. doi: 10.1016/0168-1656(94)90187-2.

**Brauer MJ**, Saldanha AJ, Dolinski K, Botstein D. Homeostatic adjustment and metabolic remodeling in glucose-limited yeast cultures. Mol Biol Cell. 2005 May; 16(5):2503–2517. doi: 10.1091/mbc.E04-11-0968.

**Bristow SL**, Leman AR, Simmons Kovacs LA, Deckard A, Harer J, Haase SB. Checkpoints couple transcription network oscillator dynamics to cell-cycle progression. Genome Biol. 2014; 15(9):446. doi: 10.1186/s13059-014-0446-7.

**Bryan AK**, Goranov A, Amon A, Manalis SR. Measurement of mass, density, and volume during the cell cycle of yeast. Proc Natl Acad Sci U S A. 2010 Jan; 107(3):999–1004.

**Burnetti AJ**, Aydin M, Buchler NE. Cell cycle Start is coupled to entry into the yeast metabolic cycle across diverse strains and growth rates. Mol Biol Cell. 2016 Jan; 27(1):64–74. doi: 10.1091/mbc.E15-07-0454.

**Causton HC**, Feeney KA, Ziegler CA, O'Neill JS. Metabolic Cycles in Yeast Share Features Conserved among Circadian Rhythms. Curr Biol. 2015 Apr; 25(8):1056–1062. doi: 10.1016/j.cub.2015.02.035.

**Chin SL**, Marcus IM, Klevecz RR, Li CM. Dynamics of oscillatory phenotypes in *Saccharomyces cerevisiae* reveal a network of genome-wide transcriptional oscillators. FEBS J. 2012 Mar; 279(6):1119–1130. doi: 10.1111/j.1742-4658.2012.08508.x.

**Christiano R**, Nagaraj N, Frohlich F, Walther TC. Global proteome turnover analyses of the Yeasts *S. cerevisiae* and *S. pombe*. Cell Rep. 2014 Dec; 9(5):1959–1965. doi: 10.1016/j.celrep.2014.10.065.

**Cookson NA**, Cookson SW, Tsimring LS, Hasty J. Cell cycle-dependent variations in protein concentration. Nucleic Acids Res. 2010 May; 38(8):2676–2681.

**Duboc P**, von Stockar U. Modeling of oscillating cultivations of *Saccharomyces cerevisiae*: Identification of population structure and expansion kinetics based on on-line measurements. Chemical Engineering Science. 2000; 55(1):149–160. doi: 10.1016/S0009-2509(99)00301-2.

**Feltham J**, Xi S, Murray S, Wouters M, Urdiain-Arraiza J, George C, Townley A, Roberts E, Fisher R, Liberatori S, Mohammed S, Kessler B, Mellor J. Transcriptional changes are regulated by metabolic pathway dynamics but decoupled from protein levels. bioRxiv. 2019; doi: 10.1101/833921.

**Futcher B**. Metabolic cycle, cell cycle, and the finishing kick to Start. Genome Biol. 2006; 7(4):107. doi: 10.1186/gb-2006-7-4-107.

**Gasch AP**, Spellman PT, Kao CM, Carmel-Harel O, Eisen MB, Storz G, Botstein D, Brown PO. Genomic expression programs in the response of yeast cells to environmental changes. Mol Biol Cell. 2000 Dec; 11(12):4241–4257.

**Geisberg JV**, Moqtaderi Z, Fan X, Ozsolak F, Struhl K. Global analysis of mRNA isoform half-lives reveals stabilizing and destabilizing elements in yeast. Cell. 2014 Feb; 156(4):812–824.

**Ghenim L**, Allier C, Obeid P, Herve L, Fortin JY, Balakirev M, Gidrol X. A new ultradian rhythm in mammalian cell dry mass observed by holography. Sci Rep. 2021 Jan; 11(1):1290. doi: 10.1038/s41598-020-79661-9.

**Hans MA**, Heinzle E, Wittmann C. Free intracellular amino acid pools during autonomous oscillations in *Saccharomyces cerevisiae*. Biotechnol Bioeng. 2003 Apr; 82(2):143–151. doi: 10.1002/bit.10553.

**Hansson L**, Häggström MH. Effects of growth conditions on superoxide dismutase and catalase activities in *Saccharomyces cerevisiae* var. ellipsoideus. Current Microbiology. 1983; 9(1):19–23. http://dx.doi.org/10.1007/BF01567128, doi: 10.1007/BF01567128.

**Heinzle E**. Mass spectrometry for on-line monitoring of biotechnological processes. In: *Biotechnology Methods* Springer; 1987.p. 1–45.

**Hereford LM**, Rosbash M. Number and distribution of polyadenylated RNA sequences in yeast. Cell. 1977 Mar; 10(3):453–462. https://doi.org/10.1016/0092-8674(77)90032-0, doi: 10.1016/0092-8674(77)90032-0.

**Hjortso MA**, Nielsen J. Population balance models of autonomous microbial oscillations. J Biotechnol. 1995 Oct; 42(3):255–269.

**Hoffmann S**, Otto C, Doose G, Tanzer A, Langenberger D, Christ S, Kunz M, Holdt LM, Teupser D, Hackermüller J, Stadler PF. A multi-split mapping algorithm for circular RNA, splicing, trans-splicing and fusion detection. Genome Biol. 2014; 15(2):R34. doi: 10.1186/gb-2014-15-2-r34.

**Jansen R**, Bussemaker HJ, Gerstein M. Revisiting the codon adaptation index from a whole-genome perspective: analyzing the relationship between gene expression and codon occurrence in yeast using a variety of models. Nucleic Acids Research. 2003 04; 31(8):2242–2251. https://doi.org/10.1093/nar/gkg306, doi: 10.1093/nar/gkg306.

**Jimeno-González S**, Payán-Bravo L, Muñoz-Cabello AM, Guijo M, Gutierrez G, Prado F, Reyes JC. Defective histone supply causes changes in RNA polymerase II elongation rate and cotranscriptional pre-mRNA splicing. Proceedings of the National Academy of Sciences. 2015; 112(48):14840–14845. https://www.pnas.org/content/112/48/14840, doi: 10.1073/pnas.1506760112.

**Jorgensen P**, Rupes I, Sharom JR, Schneper L, Broach JR, Tyers M. A dynamic transcriptional network communicates growth potential to ribosome synthesis and critical cell size. Genes Dev. 2004 Oct; 18(20):2491–2505. doi: 10.1101/gad.1228804.

**Karlsen J**, Asplund-Samuelsson J, Jahn M, Vitay D, Hudson EP. Slow Protein Turnover Explains Limited Protein-Level Response to Diurnal Transcriptional Oscillations in Cyanobacteria. Frontiers in Microbiology. 2021; 12:820. https://www.frontiersin.org/article/10.3389/fmicb.2021.657379, doi: 10.3389/fmicb.2021.657379.

**Keulers M**, Satroutdinov AD, Suzuki T, Kuriyama H. Synchronization affector of autonomous short-period-sustained oscillation of *Saccharomyces cerevisiae*. Yeast. 1996 Jun; 12(7):673–682. doi: 10.1002/(SICI)1097-0061(19960615)12:7<673::AID-YEA958>3.0.CO;2-C.

**Klevecz RR**. Quantized generation time in mammalian cells as an expression of the cellular clock. Proc Natl Acad Sci U S A. 1976 Nov; 73(11):4012–4016.

**Klevecz RR**, Bolen J, Forrest G, Murray DB. A genomewide oscillation in transcription gates DNA replication and cell cycle. Proc Natl Acad Sci U S A. 2004 Feb 3; 101(5):1200–5. doi: 10.1073/pnas.0306490101.

**Koch AL**. Why can't a cell grow infinitely fast? Can J Microbiol. 1988 Apr; 34(4):421–426.

**Krahmer J**, Hindle M, Perby LK, Mogensen HK, Nielsen TH, Halliday KJ, VanOoijen G, LeBihan T, Millar AJ. The circadian clock gene circuit controls protein and phosphoprotein rhythms in Arabidopsis thaliana. Molecular & Cellular Proteomics. 2021 Nov; .

**Kristjuhan A**, Svejstrup JQ. Evidence for distinct mechanisms facilitating transcript elongation through chromatin in vivo. The EMBO Journal. 2004; 23(21):4243–4252. https://www.embopress.org/doi/abs/10.1038/sj.emboj.7600433, doi: https://doi.org/10.1038/sj.emboj.7600433.

**Kuang Z**, Cai L, Zhang X, Ji H, Tu BP, Boeke JD. High-temporal-resolution view of transcription and chromatin states across distinct metabolic states in budding yeast. Nat Struct Mol Biol. 2014 Oct; 21(10):854–863. doi: 10.1038/nsmb.2881.

**Küenzi MT**, Fiechter A. Changes in carbohydrate composition and trehalase-activity during the budding cycle of *Saccharomyces cerevisiae*. Archives of Microbiology. 1969; 64(4):396–407. doi: 10.1007/BF00417021, 10.1007/BF00417021.

**Langdon EM**, Qiu Y, Ghanbari Niaki A, McLaughlin GA, Weidmann CA, Gerbich TM, Smith JA, Crutchley JM, Termini CM, Weeks KM, Myong S, Gladfelter AS. mRNA structure determines specificity of a polyQ-driven phase separation. Science. 2018 May; 360(6391):922–927. doi: 10.1126/science.aar7432.

**Lee W**, Tillo D, Bray N, Morse RH, Davis RW, Hughes TR, Nislow C. A high-resolution atlas of nucleosome occupancy in yeast. Nat Genet. 2007 Oct; 39(10):1235–1244. doi: 10.1038/ng2117.

**Levin JZ**, Yassour M, Adiconis X, Nusbaum C, Thompson DA, Friedman N, Gnirke A, Regev A. Comprehensive comparative analysis of strand-specific RNA sequencing methods. Nat Methods. 2010 Sep; 7(9):709–715. doi: 10.1038/nmeth.1491.

**Li CM**, Klevecz RR. A rapid genome-scale response of the transcriptional oscillator to perturbation reveals a period-doubling path to phenotypic change. Proc Natl Acad Sci U S A. 2006 Oct 31; 103(44):16254–9.

**Lindner P**. Mikroskopische Betriebskontrolle in den Gärungsgewerben: mit einer Einführung in die Hefenreinkultur, Infektionslehre und Hefenkunde, für Studierende und Praktiker bearbeitet. P. Parey; 1895. https://books.google.de/books?id=1VFIAAAAYAAJ.

**Lindner P**. Das Biosproblem in der Hefeforschung. Berichte der Deutschen Botanischen Gesellschaft. 1919; 37(11):34–40. doi: 10.1111/j.1438-8677.1919.tb07801.x.

**Litsios A**, Huberts DHEW, Terpstra HM, Guerra P, Schmidt A, Buczak K, Papagiannakis A, Rovetta M, Hekelaar J, Hubmann G, Exterkate M, Milias-Argeitis A, Heinemann M. Differential scaling between G1 protein production and cell size dynamics promotes commitment to the cell division cycle in budding yeast. Nat Cell Biol. 2019 Nov; 21(11):1382–1392. doi: 10.1038/s41556-019-0413-3.

**Liu W**, Wang J, Mitsui K, Shen H, Tsurugi K. Interaction of the GTS1 gene product with glyceraldehyde- 3-phosph ate dehydrogenase 1 required for the maintenance of the metabolic oscillations of the yeast *Saccharomyces cerevisiae*. Eur J Biochem. 2002 Jul; 269(14):3560–3569.

**Liu X**, Oh S, Peshkin L, Kirschner MW. Computationally enhanced quantitative phase microscopy reveals autonomous oscillations in mammalian cell growth. Proc Natl Acad Sci U S A. 2020 Oct; doi: 10.1073/pnas.2002152117.

**Lloyd D**, Murray DB. Redox rhythmicity: clocks at the core of temporal coherence. Bioessays. 2007 May; 29(5):465–473. doi: 10.1002/bies.20575.

**Lo K**, Hahne F, Brinkman RR, Gottardo R. flowClust: a Bioconductor package for automated gating of flow cytometry data. BMC Bioinformatics. 2009; 10:145. doi: 10.1186/1471-2105-10-145.

**Lück S**, Thurley K, Thaben PF, Westermark PO. Rhythmic degradation explains and unifies circadian transcriptome and proteome data. Cell Rep. 2014 Oct; 9(2):741–751.

**Maaløe O**. Regulation of the Protein-Synthesizing Machinery—Ribosomes, tRNA, Factors, and So On. In: Goldberger RF, editor. *Biological Regulation and Development: Gene Expression* Boston, MA: Springer US; 1979.p. 487–542. doi: 10.1007/978-1-4684-3417-0_12.

**Machné R**. Temporal Organization of Growth in *Saccharomyces cerevisiae*. PhD thesis, Theoretical Biochemistry Group, University of Vienna; 2017.

**Machné R**, Murray DB. The yin and yang of yeast transcription: elements of a global feedback system between metabolism and chromatin. PLoS One. 2012; 7(6):e37906. doi: 10.1371/journal.pone.0037906.

**Machné R**, Murray DB, Stadler PF. Similarity-Based Segmentation of Multi-Dimensional Signals. Sci Rep. 2017 Sep; 7(1):12355. doi: 10.1038/s41598-017-12401-8.

**Maharana S**, Wang J, Papadopoulos DK, Richter D, Pozniakovsky A, Poser I, Bickle M, Rizk S, Guillen-Boixet J, Franzmann TM, Jahnel M, Marrone L, Chang YT, Sterneckert J, Tomancak P, Hyman AA, Alberti S. RNA buffers the phase separation behavior of prion-like RNA binding proteins. Science. 2018 May; 360(6391):918–921. doi: 10.1126/science.aar7366.

**Marison I**, Liu JS, Ampuero S, Von Stockar U, Schenker B. Biological reaction calorimetry: development of high sensitivity bio-calorimeters. Thermochimica Acta. 1998; 309(1-2):157–173.

**Mellor J**. The molecular basis of metabolic cycles and their relationship to circadian rhythms. Nat Struct Mol Biol. 2016 Dec; 23(12):1035–1044. doi: 10.1038/nsmb.3311.

**Metzl-Raz E**, Kafri M, Yaakov G, Soifer I, Gurvich Y, Barkai N. Principles of cellular resource allocation revealed by condition-dependent proteome profiling. Elife. 2017 Aug; 6. doi: 10.7554/eLife.28034.

**von Meyenburg HK**. Energetics of the budding cycle of *Saccharomyces cerevisiae* during glucose limited aerobic growth. Archives of Microbiology. 1969; 66:289–303. doi: 10.1007/BF00414585, 10.1007/BF00414585.

**von Meyenburg K**. Katabolit-Repression und der Sprossungszyklus von *Saccharomyces cerevisiae*. PhD thesis, ETH Zürich; 1969.

**Milo R**. What is the total number of protein molecules per cell volume? A call to rethink some published values. BioEssays. 2013; 35(12):1050–1055. https://onlinelibrary.wiley.com/doi/abs/10.1002/bies.201300066, doi: https://doi.org/10.1002/bies.201300066.

**Mochan E**, Pye EK. Respiratory oscillations in adapting yeast cultures. Nat New Biol. 1973 Apr; 242(119):177–179.

**Molenaar D**, van Berlo R, de Ridder D, Teusink B. Shifts in growth strategies reflect tradeoffs in cellular economics. Mol Syst Biol. 2009; 5:323. doi: 10.1038/msb.2009.82.

**Müller D**. Model-Assisted Analysis of Cyclic AMP Signal Transduction in *Saccharomyces cerevisiae* — cAMP as Dynamic Coordinator of Energy Metabolism and Cell Cycle Progression. PhD thesis, Universität Stuttgart; 2006.

**Münch T**, Sonnleitner B, Fiechter A. The decisive role of the *Saccharomyces cerevisiae* cell cycle behaviour for dynamic growth characterization. J Biotechnol. 1992 Feb; 22(3):329–351.

**Murray DB**, Beckmann M, Kitano H. Regulation of yeast oscillatory dynamics. Proc Natl Acad Sci U S A. 2007 Feb; 104(7):2241–2246. doi: 10.1073/pnas.0606677104.

**Murray DB**, Engelen F, Lloyd D, Kuriyama H. Involvement of glutathione in the regulation of respiratory oscillation during a continuous culture of *Saccharomyces cerevisiae*. Microbiology. 1999 Oct; 145 ( Pt 10):2739–45.

**Murray DB**, Klevecz RR, Lloyd D. Generation and maintenance of synchrony in *Saccharomyces cerevisiae* continuous culture. Exp Cell Res. 2003 Jul 1; 287(1):10–5.

**Niessing D**, Jansen RP, Pohlmann T, Feldbrugge M. mRNA transport in fungal top models. Wiley Interdiscip Rev RNA. 2018 Jan; 9(1).

**Nocetti N**, Whitehouse I. Nucleosome repositioning underlies dynamic gene expression. Genes Dev. 2016 Mar; 30(6):660–672. doi: 10.1101/gad.274910.115.

**O' Neill JS**, Hoyle NP, Robertson JB, Edgar RS, Beale AD, Peak-Chew SY, Day J, Costa ASH, Frezza C, Causton HC. Eukaryotic cell biology is temporally coordinated to support the energetic demands of protein homeostasis. Nat Commun. 2020 Sep; 11(1):4706. doi: 10.1038/s41467-020-18330-x.

**O'Duibhir E**, Lijnzaad P, Benschop JJ, Lenstra TL, van Leenen D, Groot Koerkamp MJ, Margaritis T, Brok MO, Kemmeren P, Holstege FC. Cell cycle population effects in perturbation studies. Mol Syst Biol. 2014 Jun; 10:732. doi: 10.15252/msb.20145172.

**Orlando DA**, Lin CY, Bernard A, Wang JY, Socolar JE, Iversen ES, Hartemink AJ, Haase SB. Global control of cell-cycle transcription by coupled CDK and network oscillators. Nature. 2008 Jun; 453(7197):944–947. doi: 10.1038/nature06955.

**Parkhomchuk D**, Borodina T, Amstislavskiy V, Banaru M, Hallen L, Krobitsch S, Lehrach H, Soldatov A. Transcriptome analysis by strand-specific sequencing of complementary DNA. Nucleic Acids Res. 2009 Oct; 37(18):e123. doi: 10.1093/nar/gkp596.

**Paulo JA**, O'Connell JD, Everley RA, O'Brien J, Gygi MA, Gygi SP. Quantitative mass spectrometry-based multiplexing compares the abundance of 5000 *S. cerevisiae* proteins across 10 carbon sources. Journal of Proteomics. 2016; 148:85–93. https://www.sciencedirect.com/science/article/pii/S1874391916303013, doi: https://doi.org/10.1016/j.jprot.2016.07.005.

**Pu S**, Wong J, Turner B, Cho E, Wodak SJ. Up-to-date catalogues of yeast protein complexes. Nucleic Acids Res. 2009 Feb; 37(3):825–831. doi: 10.1093/nar/gkn1005.

**Quinodoz SA**, Jachowicz JW, Bhat P, Ollikainen N, Banerjee AK, Goronzy IN, Blanco MR, Chovanec P, Chow A, Markaki Y, Thai J, Plath K, Guttman M. RNA promotes the formation of spatial compartments in the nucleus. Cell. 2021; 184(23):5775–5790.e30. https://www.sciencedirect.com/science/article/pii/S0092867421012307, doi: https://doi.org/10.1016/j.cell.2021.10.014.

**Ripaud L**, Chumakova V, Antonin M, Hastie AR, Pinkert S, Korner R, Ruff KM, Pappu RV, Hornburg D, Mann M, Hartl FU, Hipp MS. Overexpression of Q-rich prion-like proteins suppresses polyQ cytotoxicity and alters the polyQ interactome. Proc Natl Acad Sci U S A. 2014 Dec; 111(51):18219–18224. doi: 10.1073/pnas.1421313111.

**Saito T**, Mitsui K, Hamada Y, Tsurugi K. Regulation of the Gts1p level by the ubiquitination system to maintain metabolic oscillations in the continuous culture of yeast. J Biol Chem. 2002 Sep; 277(37):33624–33631. doi: 10.1074/jbc.M201909200.

**Sanada M**, Kuroda K, Ueda M. ROS production and apoptosis induction by formation of Gts1p-mediated protein aggregates. Biosci Biotechnol Biochem. 2011; 75(8):1546–1553. doi: 10.1271/bbb.110226.

**Sasidharan K**, Amariei C, Tomita M, Murray DB. Rapid DNA, RNA and protein extraction protocols optimized for slow continuously growing yeast cultures. Yeast. 2012 Aug; 29(8):311–322. doi: 10.1002/yea.2911.

**Satroutdinov AD**, Kuriyama H, Kobayashi H. Oscillatory metabolism of *Saccharomyces cerevisiae* in continuous culture. FEMS Microbiol Lett. 1992 Nov; 77(1-3):261–267. doi: 10.1016/0378-1097(92)90167-m.

**Schaechter M**, Maaløe O, Kjeldgaard NO. Dependency on medium and temperature of cell size and chemical composition during balanced growth of *Salmonella typhimurium*. J Gen Microbiol. 1958 Dec; 19(3):592–606.

**Schwarz A**, Beck M. The Benefits of Cotranslational Assembly: A Structural Perspective. Trends Cell Biol. 2019 Aug; doi: 10.1016/j.tcb.2019.07.006.

**Scott M**, Gunderson CW, Mateescu EM, Zhang Z, Hwa T. Interdependence of cell growth and gene expression: origins and consequences. Science. 2010 Nov; 330(6007):1099–1102. doi: 10.1126/science.1192588.

**Shiber A**, Doring K, Friedrich U, Klann K, Merker D, Zedan M, Tippmann F, Kramer G, Bukau B. Cotranslational assembly of protein complexes in eukaryotes revealed by ribosome profiling. Nature. 2018 Sep; 561(7722):268–272. doi: 10.1038/s41586-018-0462-y.

**Slavov N**, Airoldi E, van Oudenaarden A, Botstein D. A Conserved Cell Growth Cycle Can Account for the Environmental Stress Responses of Divergent Eukaryotes. Mol Biol Cell. 2012 Mar; doi: 10.1091/mbc.E11-11-0961.

**Slavov N**, Botstein D. Coupling among growth rate response, metabolic cycle, and cell division cycle in yeast. Mol Biol Cell. 2011 Jun; 22(12):1997–2009. doi: 10.1091/mbc.E11-02-0132.

**Slavov N**, Macinskas J, Caudy A, Botstein D. Metabolic cycling without cell division cycling in respiring yeast. Proc Natl Acad Sci U S A. 2011 Nov; 108(47):19090–19095. doi: 10.1073/pnas.1116998108.

**Sonnleitner B**, Rothen SA, Kuriyama H. Dynamics of glucose consumption in yeast. Biotechnol Prog. 1997 Jan; 13(1):8–13. doi: 10.1021/bp960094+.

**Thaben PF**, Westermark PO. Detecting rhythms in time series with RAIN. J Biol Rhythms. 2014 Dec; 29(6):391–400. doi: 10.1177/0748730414553029.

**Tu BP**, Kudlicki A, Rowicka M, McKnight SL. Logic of the yeast metabolic cycle: temporal compartmentalization of cellular processes. Science. 2005 Nov 18; 310(5751):1152–8.

**Turing AM**. The Chemical Basis of Morphogenesis. Philosophical Transactions of the Royal Society of London Series B, Biological Sciences. 1952; 237(641):37–72. http://www.jstor.org/stable/92463, doi: 10.2307/92463.

**Verduyn C**, Stouthamer AH, Scheffers WA, van Dijken JP. A theoretical evaluation of growth yields of yeasts. Antonie Van Leeuwenhoek. 1991 Jan; 59(1):49–63.

**Waldron C**, Lacroute F. Effect of growth rate on the amounts of ribosomal and transfer ribonucleic acids in yeast. J Bacteriol. 1975 Jun; 122(3):855–865.

**Wang GZ**, Hickey SL, Shi L, Huang HC, Nakashe P, Koike N, Tu BP, Takahashi JS, Konopka G. Cycling Transcriptional Networks Optimize Energy Utilization on a Genome Scale. Cell Rep. 2015 Dec; 13(9):1868–1880. doi: 10.1016/j.celrep.2015.10.043.

**Wang J**, Mitsui K, Tsurugi K. The GTS1 gene product influences the ultradian oscillation of glycolysis in cell suspension of the yeast *Saccharomyces cerevisiae*. Biochem Biophys Res Commun. 1998 Mar; 244(1):239–242. doi: 10.1006/bbrc.1998.8138.

**Wang Y**, Song L, Liu M, Ge R, Zhou Q, Liu W, Li R, Qie J, Zhen B, Wang Y, He F, Qin J, Ding C. A proteomics landscape of circadian clock in mouse liver. Nature Communications. 2018 Apr; 9(1):1553.

**Xu Z**, Yaguchi S, Tsurugi K. Gts1p stabilizes oscillations in energy metabolism by activating the transcription of TPS1 encoding trehalose-6-phosphate synthase 1 in the yeast *Saccharomyces cerevisiae*. Biochem J. 2004 Oct; 383(Pt 1):171–178. doi: 10.1042/BJ20040967.

**Zenklusen D**, Larson DR, Singer RH. Single-RNA counting reveals alternative modes of gene expression in yeast. Nature Structural & Molecular Biology. 2008 Dec; 15(12):1263–1271. https://doi.org/10.1038/nsmb.1514, doi: 10.1038/nsmb.1514.